Marine Chemistry 214 (2019) 103662

Contents lists available at ScienceDirect

Marine Chemistry

journal homepage: www.elsevier.com/locate/marchem

# Assessing nutrient dynamics in mangrove porewater and adjacent tidal creek using nitrate dual-stable isotopes: A new approach to challenge the Outwelling Hypothesis?

Pierre Taillardat[a,b,*], Alan D. Ziegler[a], Daniel A. Friess[a], David Widory[b], Frank David[c], Nobuhito Ohte[d], Takashi Nakamura[e], Jaivime Evaristo[f], Nguyen Thanh-Nho[g], Truong Van Vinh[h], Cyril Marchand[i]

[a] Department of Geography, National University of Singapore, 1 Arts Link, Singapore 117570, Singapore
[b] GEOTOP, Université du Québec à Montréal, Montréal, Canada
[c] BOREA Biologie des Organismes et Ecosystèmes Aquatiques, UMR 7208 MNHN CNRS SU UA UCN IRD 207, Muséum National d'Histoire Naturelle, Paris, France
[d] Biosphere Informatics Laboratory, Kyoto University, Kyoto, Japan
[e] Interdisciplinary Centre for River Basin Environment, Yamanashi University, Japan
[f] Copernicus Institute of Sustainable Development, Utrecht University, Utrecht, the Netherlands
[g] Faculty of Environmental and Food Engineering, Nguyen Tat Thanh University, Vietnam Department, University of Sciences of Ho Chi Minh City, Viet Nam
[h] Nong Lam University, Linh Trung, Thu Duc, Ho Chi Minh City, Viet Nam
[i] Université de la Nouvelle-Calédonie, ISEA, Noumea, New Caledonia, France

A B S T R A C T

The importance of mangrove-derived material in sustaining coastal food webs (i.e. the Outwelling Hypothesis) is often invoked in support of mangroves conservation. Biogeochemical cycling, particularly nitrogen (N) and phosphorus (P) in mangrove ecosystems, however, is poorly understood because of high spatial heterogeneity and temporal variability of sources, sinks, and transformation pathways. Here we show that the distribution of N and P are intimately related to vegetation distribution, tidal cycles, and seasonality. We examined the dynamics of N and P in sediments and in a tidal creek of the Can Gio Mangrove Forest, Vietnam. Our objectives were to (1) determine the spatial distribution of dissolved inorganic nitrogen and phosphorus in the mangrove forest along a *Rhizophora-Avicennia*-mudflat transect; and (2) identify the respective inputs and transformation pathways of N and P in the water column via 24-h time series measurements in a tidal creek. Sediment porewater had $N\text{-}NH_4^+$ and $N\text{-}NO_3^-$ concentrations < 11 μM, except in the mudflat where $N\text{-}NH_4^+$ was as high as 162 μM. This difference was likely due to $N\text{-}NH_4^+$ uptake by trees in the vegetated areas and suggests that mangrove sediments can be a zone of $NH_4^+$ production via ammonification of organic nitrogen. In all stands, $P\text{-}PO_4^{3-}$ concentrations were three-fold higher during the wet season, with a maximum of 34.4 μM. This can be explained by enhanced microbial activity during the rainy season. The phosphorus seasonal trend was also observed in the creek water but with a maximum $P\text{-}PO_4^{3-}$ value of 4.3 μM only. In the tidal creek, $N\text{-}NH_4^+$ was highly variable (0 to 51 μM), with the higher values measured at low tide and related to porewater discharge from the mudflat. Our data suggest that mangroves act both as a sink of dissolved inorganic nutrients via vegetation uptake and a source of ammonium from unvegetated mudflat porewater towards the tidal creek. The dual stable isotopes approach ($\delta^{15}N_{NO3}$ & $\delta^{18}O_{NO3}$) revealed that this ammonium was later nitrified within the water column. Moreover, the approach showed that some nitrate originated from the river-estuarine system during rising tides. The export of ammonium from mangrove porewater is presumably entirely consumed before exiting the tidal creek, thereby limiting the spatial extent of mangrove Outwelling. Nevertheless, our multi-isotope approach leads us to conclude that nutrients recycling via mangrove-derived organic matter mineralization may play a fundamental role in sustaining coastal food web.

## 1. Introduction

Mangrove ecosystems are intertidal forests with contiguous waterways that develop on warm-temperate, subtropical, and tropical coastlines. They are among the most productive ecosystems on Earth, even though they are naturally nutrient-limited (Alongi, 2009; Alongi, 2018). The unique coastal conditions in which they exist mean that mangrove vegetation has adapted to salinity, reducing conditions, periodic tidal forcing, and inundation (Reef et al., 2010). This environmental setting directly influences mangrove ecosystem productivity and nutrient availability (Twilley et al., 2017). Fast changing environmental conditions and spatial heterogeneity along the elevation gradient makes the cycling of nitrogen (N) and phosphorus (P), identified as two limiting nutrients in mangroves (Reef et al., 2010), complex and rapidly changing.

Nutrient tidal exchange and mangrove connectivity with coastal

* Corresponding author.
*E-mail address:* taillardat.pierre@courrier.uqam.ca (P. Taillardat).

https://doi.org/10.1016/j.marchem.2019.103662
Received 4 March 2019; Received in revised form 16 May 2019; Accepted 24 May 2019
Available online 03 June 2019
0304-4203/ 

waters share a long history in the ecological literature. For example, the Outwelling Hypothesis, proposed by Odum (1968) for saltmarshes, and discussed since then for mangrove habitats (Boto and Bunt, 1981; Bouillon et al., 2011; Lee, 1995; Odum and Heald, 1975), suggests that coastal wetlands export organic matter (OM) and nutrients to surrounding waters. This export is presumed to support aquatic productivity, eventually after transformation into available forms. Low nutrient concentrations and rapid nutrient transformations in temporally dynamic and spatially heterogeneous intertidal zones, however, pose a challenge to mass balance calculations that are necessary for testing this hypothesis. To date, only one study has done so (Alongi, 2013), which highlights the need to better constrain nutrient fluxes and transformation processes.

The largest nutrient pool in mangrove ecosystems is the soil (Alongi, 2018). Most of the organic nutrients present in the soil nutrient pool system are from the mangrove vegetation itself, via litterfall as particulate organic nutrients on the mangrove floor or in the belowground roots as dissolved organic nutrient exudates in the sediment porewater (Alongi, 2013; Kristensen and Alongi, 2006; Kristensen et al., 1995). Feces, dead animals, microbial mixture, and tidal import can also account for a secondary pool of organic matter (Adame et al., 2010; Alongi, 2013; David et al., 2018). When this organic material accumulates in the sediment or becomes buried by crab burrowing, mineralization occurs and releases inorganic nutrients that are bioavailable for vegetation uptake (Feller et al., 2003). Ammonium, the product of organic nitrogen mineralization (i.e. ammonification), is the predominant N species in mangrove soils (Alongi, 2018; Sherman et al., 1998). It is also the form preferentially assimilated by mangrove vegetation, incorporated by the large belowground root network (Reef et al., 2010). Soil processes and characteristics, such as the intensity of bioturbation, radial oxygen loss from roots, and grain size fraction can influence the soil redox potential and therefore the nutrient biogeochemical transformation pathways and nutrient availability for plants (Reef et al., 2010). Based on a mass balance assessment, Alongi (2013) determined that soil ammonification, nitrification, and dissimilatory nitrate reduction to ammonia (DNRA) are the most important N transformation processes in mangrove soils, rather than atmospheric $N_2$ fixation and denitrification. Regarding phosphorus, $PO_4^{3-}$ immobilization in the sediment (e.g. by iron hydroxides and oxyhydroxides) is an important process that inhibits direct vegetation uptake (Alongi et al., 2002). Available phosphate is only released during the iron oxide reduction process (Deborde et al., 2015; Reef et al., 2010). Rapid uptake, constant transformation processes, and tight interaction between the organic and inorganic fractions limit our understanding of nutrient cycling in mangrove sediments. This complex matrix of organic carbon-rich mangroves soils with high porosity from animal burrows also favors strong tidal exchanges (Stieglitz et al., 2013; Tait et al., 2016).

The role of tidal exchange in the N and P dynamics is still ambiguous despite having identified environmental parameters such as latitude, temperature, rainfall, geomorphological settings, hydrology, and vegetation species that influence the direction and magnitude of nutrients exchange (Adame and Lovelock, 2011; Adame et al., 2010). Moreover, the response of mangroves in anthropogenically nutrient-enriched estuarine systems is still not clear. Some studies have suggested that mangroves act as a biofilter that attenuates eutrophication (Molnar et al., 2014; Reef et al., 2010). Others described mangroves as a direct source of nutrient for coastal waters (Dittmar et al., 2006; Tanaka and Choo, 2000). Regarding the Outwelling Hypothesis, it is now established that part of the atmospheric $CO_2$ fixed by mangrove vegetation is exported to coastal waters as dissolved organic and inorganic carbon from porewater discharge (Call et al. 2019a; Maher et al., 2018; Santos et al., 2019; Taillardat et al., 2018a). Tidal export of nutrients via the same mechanism, however, remains unclear, probably because of lower concentration ranges, the importance of recycling processes over nutrient inputs, and quick biogeochemical transformation processes of N and P forms. In addition to low concentrations and high temporal dynamics of the system, spatial heterogeneity such as distance to coastal waters or size of the hydrological unit (i.e. tidal creek) affect the nutrients net tidal exchange. Estimates have sometimes been contradictory between study sites and seasons (Dittmar and Lara, 2001a; Leopold et al., 2017; Rivera Monroy et al., 2007; Tait et al., 2017) and inconsistent with tidal variations for some elements such as phosphorus and nitrate (Gleeson et al., 2013; Ovalle et al., 1990). Some studies that investigated nutrient exchange in mangroves have been based on complete tidal cycle time series, using concentration variations as a proxy for tidal exchange rather than direct nutrient fluxes (e.g. Leopold et al., 2017; Wang et al., 2019). This underlines the challenge of accounting for elements that are quickly changing in forms and concentrations. In fact, our understanding of nutrient cycling in mangroves is still poorly understood despite being prerequisite to calculating mass balance budgets.

The aim of this study was to characterize the N and P origin, distribution, and transformation pathways in mangrove sediments and in the adjacent tidal creek in the Can Gio Mangrove Forest, Vietnam. We tested two hypotheses:

(i) N and P concentrations and distribution in mangrove sediment porewaters greatly differ among habitats and between seasons because of variability in biotic factors and abiotic conditions. Regarding the spatial variability, we expected dissolved inorganic nutrient concentrations in porewater to be lower below vegetation than in the mudflat because of tree uptake. Regarding the seasonal variability, we expected higher concentrations during the wet season because of greater water turnover and lower salinity;
(ii) Nutrient loads in the tidal creek greatly differ between tidal cycles and seasons because of the multiple origins of nutrients and intense recycling, assimilation, and transformation in the water column. Regarding nutrients origin present in the tidal creek water column, we expected that mangrove forest was a direct input at low tide via surface and subsurface discharge and that the river estuarine system was a direct input at high tide via tidal import. Regarding the recycling and transformation processes, we expected that the nutrient pool throughout a complete tidal cycle was quickly changing due to in situ processes such as uptake, nitrification, denitrification, and external input.

We tested these hypotheses by combining the use of dual nitrate stable isotopes ($\delta^{15}N_{NO3}$ & $\delta^{18}O_{NO3}$) with particulate $\delta^{13}C$ and $\delta^{15}N$. The dual nitrate stable isotope approach has contributed to identifying nitrate dynamics in various environments including estuaries and coastal waters via the discrimination of natural abundance isotope ratios as indicators of organic matter origin, production, consumption and degradation processes (Archana et al., 2018; Wankel et al., 2009; Xue et al., 2014). However, it has not yet been used directly to document nitrogen cycling in complex intertidal mangrove systems except in one disturbed subtropical mangrove tidal creek (Wang et al., 2019). Conversely, stable isotopes ($\delta^{13}C$ and $\delta^{15}N$) of particulate organic matter have been applied in mangroves to help understand ecosystem functioning including delineation of organic matter and nutrient sources in different pools and transformation processes leading to isotopic fractionation (Bouillon et al., 2008). In this study, we combined the use of nitrate dual-stable isotopes with particulate $\delta^{13}C$ and $\delta^{15}N$ to generate new insights on mangrove nutrient cycling.

## 2. Methods

### 2.1. Study site

The protected Can Gio mangrove forest (Fig. 1) is located 35 km southeast of Ho Chi Minh City, the most populated city (> 8 million inhabitants) and economic center of Vietnam (UN, 2014). The city is

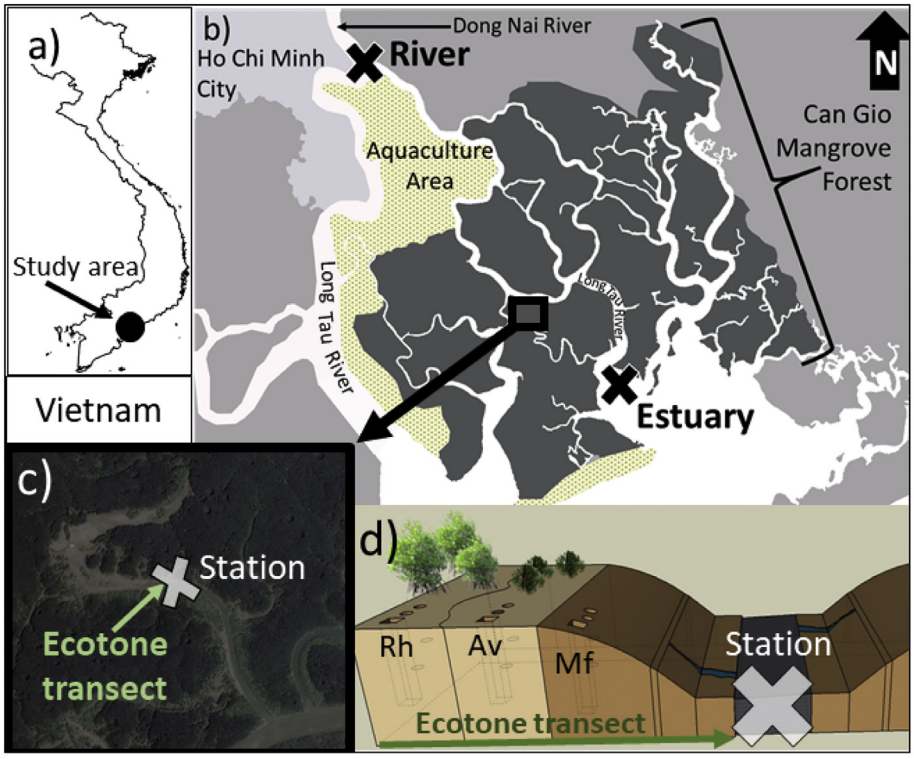


**Fig. 1.** (a) Map of Vietnam, with the black dot representing the location of the study area; (b) Map of the Can Gio Mangrove UNESCO Biosphere Reserve study area and its surroundings, where the light gray colour represents Ho Chi Minh City, the yellow background with black dots is the aquaculture area, the dark gray is the mangrove UNESCO Biosphere Reserve area, and the black square represents the study site. The two black crosses represent the river and estuary end-members as described in the text; (c) Map of the mangrove tidal creek study site, with the gray cross representing the time series monitoring station and the green arrow the ecotone transect; (d) Conceptual model of the tidal creek with "Rh" for *Rhizophora*-dominated ecotone, "Av" for *Avicennia*-dominated ecotone and "Mf" for mudflat. (For interpretation of the references to colour in this figure legend, the reader is referred to the web version of this article.)

hydrologically connected to the Can Gio mangrove forest via the Dong Nai River, which originates in the Central Highlands and is approximately 600 km long (Grayman et al., 2003). Land uses within the catchment area of ≈ 36,000 $km^2$ are predominantly (1) agriculture upstream of Ho Chi Minh City; (2) urban and industrial areas within the Ho Chi Minh City municipality; (3) aquaculture downstream of the city; and finally (4) the Can Gio Mangrove UNESCO Biosphere Reserve (Fig. 1). We studied a tidal creek approximately 1400 m long, located in the middle of the Can Gio Mangrove Forest (10 30.339′N; 106 52.943′E), with no direct surface freshwater input other than rainfall (Fig. 1). The site exhibited an ecotone progression composed of *Rhizophora*-dominated land cover, *Avicennia*-dominated land cover and a mudflat area, from the forest core to the tidal creek, which is the typical distribution along the elevation gradient in the Can Gio mangrove (Fig. 1d).

The mangrove forest in Can Gio covers about 38,000 ha (Kuenzer and Tuan, 2013) and was partially destroyed by the spraying of herbicides and other chemical agents during the 1961–1971 Vietnam-USA War (Nam et al., 2014). The mangrove was rehabilitated via multiple replantation programs from 1978 onwards (Le, 2008). The mangrove forest is dominated by replanted and naturally regenerating *Rhizophora apiculata*. Additionally, *Avicennia alba* has naturally recolonized the edge of the tidal creeks (Dung et al., 2016; Kuenzer and Tuan, 2013). We also identified *A. officinalis, A. marina, A. rumphiana*, and *Sonneratia alba* during our field surveys. The Can Gio mangrove forest is now mature with vegetation distribution, diversity, and above-ground carbon stocks comparable to other low-latitude mangroves in South East Asia (Arnaud-Haond et al., 2009; Van Vinh et al., 2019).

The dry season in the study area occurs from late October to early May and the wet season from early May until the end of October. Annual temperature and precipitation range between 26.5 and 30.0 °C and between 1600 and 2250 mm, respectively, with ~64% of the precipitation occurring during the wet season (Le, 2008). The tidal regime is characterized by a strong diurnal inequality (Conley, 2015) with tidal oscillations changing from symmetric (semi-diurnal tide) to asymmetric (diurnal tide) over a full cycle (≈ 24 h 50 min). The mean tidal amplitude is 2.3 m and the creek bank elevation is ≈ 1.9 m relative to the lowest topographical point in the middle of the tidal creek (Taillardat et al., 2018b).

### 2.2. Field measurements

Time series measurements of 24-h were performed from an anchored boat located in the middle of the tidal creek (Fig. 1c) during the asymmetric and symmetric tidal cycles for each season (i.e. 7 pm 12/04/2015 to 6 pm 13/04/2015 and 12 pm 18/04/2015 to 12 pm 19/04/2015 for the dry season; 3 pm 19/10/2015 to 3 pm 20/10/2015 and 11 am 26/10/2015 to 11 am 27/10/2015 for the wet season). Tidal amplitude for each tidal cycle was always greater than the creek bank height of 1.94 m, meaning that coastal waters were flowing into the mangrove forest daily. Fig. 2 is an illustration of tidal oscillation in the study site with the water creek bank as a reference point.

Salinity, water temperature, and pH were recorded every 5 min using a calibrated Yellow Springs Instrument (YSI) 6920 multi-parameter probe. Dissolved oxygen (DO) was measured using a calibrated Hobo U26–001 dissolved oxygen data logger. Concentrations of the 222-Radon radioisotope ($^{222}Rn$) were measured in water during the wet season only, using the showerhead equilibration technique. Briefly, creek water was continuously pumped to an equilibration chamber where the head-space gas was streamed into an automated $^{222}Rn$-in-air analyzer using the Rad Aqua package (RAD7, Durridge Co.; Burnett et al., 2001). Discrete surface water samples were collected every 2 h (13 samples per 24-h time series) using a bucket (at ~0.3 m depth). All samples (~100–400 mL) were filtered through pre-weighed and pre-combusted (4 h, 400 °C) glass fiber filters (Whatman GF/F 0.7 μm, 47 mm diameter) that were later used for determining suspended particulate matter (SPM), particulate organic carbon (POC), particulate nitrogen (PN), $\delta^{13}C_{POC}$, and $\delta^{15}N$. The filtered water was stored in 15 mL PP tubes kept in a cooler until taken back to the city where they were frozen until they were analyzed for $N\text{-}NH_4^+$, $N\text{-}NO_3^-$, $N\text{-}NO_2^-$, $P\text{-}PO_4^{3-}$, $\delta^{15}N_{NO3}$ & $\delta^{18}O_{NO3}$. Unfiltered samples for water $\delta^{18}O$ and $\delta^{2}D$ were kept in 4 mL, fully-filled tubes with no air bubble, and sealed with parafilm.

During the two seasons, mangrove sediments and porewaters were

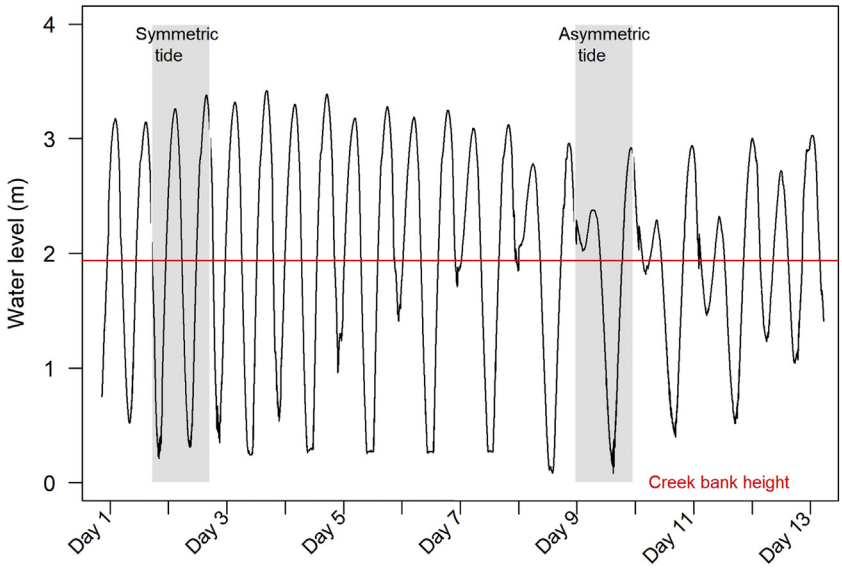


**Fig. 2.** Typical tidal oscillation in the Can Gio Mangrove Forest under a tidal regime of strong diurnal inequality over a half lunar tidal cycle (14 days). Periods highlighted in gray are the two time series presented in this study accounting for the symmetric and asymmetric tidal cycles for each season (total = 4 time series). The red line represents the creek bank height at the station. When the water level is higher than this line, the mangrove forest is being flooded. (For interpretation of the references to colour in this figure legend, the reader is referred to the web version of this article.)

collected at low tide across a representative ecotone transect, extending from the mangrove forest to the tidal creek, i.e. from the *Rhizophora*-dominated mangrove through the *Avicennia*-dominated zone to the mudflat (Fig. 1). For porewater three ≈ 60 cm depth bore holes were excavated with a shovel in each of the three habitats. The water in bores was purged three times before porewater was collected via a suction tube (Taillardat et al., 2018a). Porewater samples conservation and preparation followed the same protocol as for surface water sampling (see above) for the analysis of $N\text{-}NH_4^+$, $N\text{-}NO_3^-$, $N\text{-}NO_2^-$, $P\text{-}PO_4^{3-}$, $\delta^{15}N_{NO3}$ & $\delta^{18}O_{NO3}$, and $\delta^{18}O$ & $\delta^2H$.

For sediment samples, triplicate cores of 1 m were taken using an Eijkelkamp gouge auger at a distance < 50 cm of the porewater bores. The pH and Oxidation-Reduction Potential (ORP) were determined in the field using an ORP meter (YSI during the dry season, Wissenschaftlich-Technische-Werkstätten during the wet season) at 5 cm intervals on the sediment core until reaching 70 cm depth, where measurements were taken every 10 cm until 100 cm depth. ORP is reported as relative to a standard hydrogen electrode by adding the mV correction based on the Ag/AgCl reference type and the sample temperature (Lenton and Watson, 2000; Striggow, 2017). Fresh leaves of *R. apiculata* and *A. alba* were collected during both seasons. Sediment and leaf samples were brought back to the laboratory and kept frozen until analyzed (%OC, %N, $\delta^{13}C$, $\delta^{15}N$).

Finally, river and estuary water samples (upstream and downstream the mangrove) were collected following the same protocols as for surface water samples in the tidal creek. The locations of the identified end-members are presented in Fig. 1b.

### 2.3. Solid-phase laboratory analyses

Grain size fractions were determined using a Mastersizer 2000 particle size analyzer (Malvern Instruments). Values were measured at 5 cm intervals on the sediment core until reaching 70 cm depth where measurements were taken every 10 cm until 100 cm depth.

Filters and sediments for organic carbon, particulate nitrogen, $\delta^{13}C$, and $\delta^{15}N$ were freeze-dried overnight. For the organic carbon analysis, filters were also fumigated for 24-h under an air-tight glass bell containing three beakers of ~10 mL of HCl (12 N) to remove inorganic carbon (e.g. Hélie, 2009). Organic carbon percentage (%OC) and nitrogen percentage (%N) were determined using an elemental analyzer (NC instruments NC2500™). The $\delta^{13}C$ and $\delta^{15}N$ on sediments and filters were measured using an elemental analyzer (Vario Micro Cube™) coupled to an Isoprime 100™ IRMS in continuous flow mode at the Geotop laboratory (Université du Québec à Montréal, Canada). Replicated $\delta^{13}C$ and $\delta^{15}N$ measurements from selected samples yielded an overall analytical error of ± 0.1‰.

### 2.4. Dissolved-phase laboratory analyses

Nutrient concentrations ($N\text{-}NH_4^+$, $N\text{-}NO_2^-$, $N\text{-}NO_3^-$, $P\text{-}PO_4^{3-}$) were measured using a Flow Injection Analyzer (FIA, Lachat). Values of $\delta^{18}O$ and $\delta^2H$ of $H_2O$ were performed using isotope ratio infrared spectroscopy (LGR OA-ICOS CA, USA) at McDonnell Watershed Hydrology Lab, Canada. Laboratory precision was ± 1‰ and ± 0.2‰ for $\delta^2H$ and $\delta^{18}O$, respectively. The $\delta^{15}N_{NO3}$ and $\delta^{18}O_{NO3}$ values were determined using the bacterial denitrification method (Sigman et al., 2001) at the Interdisciplinary Centre for River Basin Environment (ICRE, Yamanashi University, Japan). The bacterial denitrification method consists of converting the dissolved $N\text{-}NO_3$ into $N_2O$ using denitrifying bacteria that lack $N_2O$-reductase activity. Corresponding isotope compositions, $\delta^{15}N_{NO3}$ and $\delta^{18}O_{NO3}$, were measured using a Sercon CryoPrep trace gas concentration system interfaced to a Sercon Isotope-Ratio Mass Spectrometer (Crewe, United Kingdom). The $N_2O$ samples are purged from vials through a double-needle sampler using a helium carrier stream (~6 p.s.i., 15 mL/min.). Both $CO_2$ and $H_2O$ are removed from the gas stream using Carbosorb™ and magnesium perchlorate reagents. By cryogenic trapping and focusing, the $N_2O$ is compressed onto two Capillary GC columns: a 10 m × 0.53 mm ID Molesive 5A at 40 °C for separating primary gases ($N_2$ and $O_2$), followed by a 10 m × 0.32 mm ID PoraPLOT-Q at 40 °C for separating trace gases ($CO_2$ and $N_2O$). Subsequently, samples are analyzed by isotope ratio mass spectrometry (IRMS). Stable isotope compositions are expressed in delta (δ) units in permil (‰) relative to the respective international standards:

$$\delta\left({}^{i}_{j}E\right)(\text{in‰}) = \left[\frac{N({}^{i}E)_p / N({}^{j}E)_p}{N({}^{i}E)_{std} / N({}^{j}E)_{std}}\right] - 1.$$

where $N({}^{i}E)_p$ and $N({}^{j}E)_p$ are the amounts of the two isotopes ${}^{i}E$ and ${}^{j}E$ of chemical element E in specimen P; and equivalent parameters follow for the international measurement standard, 'std' (Coplen, 2011). As described in Brand et al. (2014), we have simplified the notation to $\delta^{i}E$. $\delta^{15}N_{NO3}$ and $\delta^{18}O_{NO3}$ measurements are given relative to atmospheric air and standard mean ocean water (VSMOW), respectively. The raw data are corrected with the aid of a calibration curve constructed from the isotope analysis of the following certified standards: USGS 32, USGS 34, USGS 35, Dry $N_2O$, and IAEA ($KNO_3$) for $\delta^{15}N_{NO3}$ and $\delta^{18}O_{NO3}$.

### 2.5. Nutrient ratio, excess and removal

The N:P ratio was calculated for each sample. This ratio was compared to the Redfield ratio, which is a fixed value of DIN:DIP = 16:1 based on phytoplanktonic biomass (Redfield, 1958). The Redfield ratio is commonly used to understand biological processes in marine environments (Lenton and Watson, 2000) and also to discuss terrestrial ecosystems productivity (McGroddy et al., 2004).

Additionally, we assessed enrichment/removal of N-$NO_3^-$ with the quasi-conservative tracer N* described by Gruber and Sarmiento (1997) from a linear combination of nitrate and phosphate for all samples (porewater and surface water sample):

$$N* = N - NO_3^- - 16\,x\,P - PO_4^{3-} + 2.9 \quad (1)$$

where units are μM; N* > 0 suggests an excess of N-$NO_3^-$ (by external source, nitrification, or N fixation); whereas N* < 0 suggests an overall removal of N-$NO_3^-$ (by denitrification or assimilation).

### 2.6. Nitrification determination

The study of $\delta^{18}O_{NO3}$ isotope compositions can help in determining if (and how) the nitrification process occurred (Kendall et al., 2007). Nitrification is a biologically-mediated reaction that induces N and O isotope fractionation. For oxygen, the $\delta^{18}O$ of the $NO_3$ formed by nitrification results in an isotope balance between the two oxidant sources: two oxygen atoms and their corresponding $\delta^{18}O$ taken from the water and one from the air (Kendall et al., 2007; Lu et al., 2015). We compared the values measured in our samples with those calculated using the $\delta^{18}O_{O2}$ from the atmosphere at 23.5 ± 0.3‰ (Kroopnick and Craig, 1972) and the locally measured $\delta^{18}O_{H2O}$ from water sample (here, porewater and the tidal creek surface water).

### 2.7. Statistical analysis

Nutrient concentrations and stable isotope compositions were compared using the non-parametric Wilcoxon test (W). Multiple comparisons were done using the non-parametric Kruskal-Wallis rank sum test (H) and significant differences were highlighted using pairwise Wilcoxon comparisons. We used nonparametric tests as the small sample size did not yield data that were normally distributed.

## 3. Results

### 3.1. Sediment characteristics and nutrient concentrations in porewater along the ecotone transect

#### 3.1.1. Sediment characteristics along the ecotone transect

Total organic carbon content and sediment particle size were distinct between the three habitats but homogeneous with depth in each stand (Fig. 3). A significantly higher total organic carbon content ($H_{3,42}$ = 31.174; $p$ < .001) was measured in the *Rhizopohora* stand (median [min; max] 6.7% [4.1; 9.0]) compared with the *Avicennia* stand (2.3% [1.1; 3.4]) and the mudflat (2.3% [2.1; 2.6]) (Fig. 3). The main difference in the grain size fractions was related to sand content. About 15% of the sediment at the *Rhizophora* stand was composed of sand, which was much higher than in the mudflat (4%) and the *Avicennia* stand (2%) (Fig. 3). The clay fraction was within the same order of magnitude between the three sites, ranging from 7 to 9%. Silt was the dominant grain size fraction: up to 78% in the *Rhizophora* stand, 90% in the *Avicennia* stand, and 88% in the mudflat (Fig. 3).

The sediment pH values were similar between seasons in both *Rhizophora* (6.4 [6.2; 6.6]) and *Avicennia* (6.4 [5.5; 5.8]) stands, but they were significantly lower ($H_{3,93}$ = 62.6; $p$ < .001) than in the mudflat (6.9 [6.7; 7.1]) (Fig. 3). The ORP conditions across the three ecotones ranged from −185 (reducing conditions) to 265 mV (oxidizing conditions), with high variability between triplicates (Fig. 3). Reducing conditions increased with depth in the sediments. In the *Rhizophora* stand, the ORP values decreased rapidly during the dry season: the sediment was oxidizing (> 80 mV) in the upper 5 cm; suboxic (0 to 80 mV) from 5 to 15 cm depth; then reducing (< 0 mV) until the bottom of the core (1 m) (Fig. 3). During the wet season, the sediment in the *Rhizophora* stand oscillated from suboxic to anoxic conditions for the same depth, with values overall reducing significantly less (i.e. ORP values higher) than during the dry season ($W_{2,30}$ = 16; p < .001). In the sediments under the *Avicennia* vegetation, the ORP steadily decreased with depth during both seasons, with no significant seasonal difference ($W_{2,30}$ = 144; $p$ = .5586); and an overall reducing state reached below 50 cm depth (Fig. 3). The mudflat conditions were predominantly suboxic during the dry season (17.8 mV [2.7; 117]), with values significantly more reduced ($W_{2,30}$ = 52; $p$ < .005) than during the wet season (83.5 mV [10; 177]; Fig. 3).

The median [min; max] sediment isotope compositions were − 27.1‰ [−29.4; −26.4] for $\delta^{13}C$ and 4.6‰ [1.9; 7.9] for $\delta^{15}N$. The median fresh mangrove vegetation isotope compositions were − 29.0‰ [−33.3; −26.7] for $\delta^{13}C$ and 6.9‰ [2.3; 12.2] for $\delta^{15}N$.

#### 3.1.2. Nutrient concentrations in porewater along the ecotone transect

Most of the porewater dissolved inorganic nitrogen (DIN) measured in this study was ammonium (N-$NH_4^+$) (Fig. 4 and Table 1). However, there were significant variations between stands ($H_{3,39}$ = 22.87; p < .001), with N-$NH_4^+$ values 5 to 6-fold higher in the mudflat (21.1 μM [0.6; 162.4]) compared to the *Rhizophora*-dominated (3.0 μM [1.7; 5.3]) and *Avicennia*-dominated (4.3 μM [1.0; 6.0]) stands (Fig. 4 and Table 1). Nitrite (N-$NO_2^-$) was almost always absent in porewater with a median value of 0.0 μM, and a maximum concentration of 3.8 μM (Fig. 4). Nitrate (N-$NO_3^-$) concentrations, ranging from 0 to 10.7 μM, did not differ between the three stands ($H_{3,29}$ = 1.03; $p$ = .7949), but significantly higher values were measured during the dry season ($W_{2,30}$ = 64.5; $p$ < .05) (Fig. 4). N-$NO_3^-$ concentrations were within the same order of magnitude than N-$NH_4^+$ in *Rhizophora* and *Avicennia* stands (< 11 μM), but much lower than N-$NH_4^+$ in the mudflat porewater (Fig. 4).

Similar to nitrate, phosphate concentrations, ranging from 0.2 to 34.4 μM, did not differ between the three stands ($H_{3,39}$ = 0.93; $p$ = .6268) but were three-fold higher values during the wet season in all stands, ranging from 0.2 to 34.4 μM (Fig. 4). Median values of P-$PO_4^{3-}$were 5.0 μM [2.4; 34.4], 5.2 μM [3.5; 13.5], 3.6 μM [2.7; 14.9] for the *Rhizophora* stand, the *Avicennia* stand, and the mudflat, respectively, during the wet season; and 1.8 μM [1.5; 1.9], 1.8 μM [1.6; 2.0], and 1.3 μM [0.2; 1.7], respectively, during the dry season (Fig. 4).

Despite seasonal variability in P-$PO_4^3$, nitrogen appeared to be the limiting nutrient in mangrove porewater as the median DIN:DIP ratio was 2.9:1 [0.1:1; 48.2:1]. Only mudflat porewater during the wet season showed a P-limited environment with a median ratio of 33.6:1 [16.5:1; 48.2:1]. The N* was constantly > 0 [0.6; 134.4], suggesting that nutrient input from $N_2$ fixation or organic matter mineralization was always greater than its uptake from autotrophic and heterotrophic organisms.

No significant differences were measured for $\delta^{15}N_{NO3}$ ($H_{3,11}$ = 1.5715; $p$ = .6659) and $\delta^{18}O_{NO3}$ ($H_{3,11}$ = = 3.5171; $p$ = .31859) in porewater between the three stands, with values ranging from − 0.9‰ to 12.7‰ for $\delta^{15}N_{NO3}$ and from − 3.9‰ to 26.62‰ for $\delta^{18}O_{NO3}$. Differences were however measured for $\delta^{18}O_{NO3}$ in porewater, with values under the *Rhizophora* stand (5.4‰ [−3.9; 19.3]) lower than under the *Avicennia* stand (14.5‰ [6.5; 23.9]) and in the mudflat (12.3‰ [0.6; 26.6]) (Table 1).

### 3.2. Nutrient dynamics in the mangrove tidal creek

Ammonium, $^{222}Rn$, and PN concentrations revealed a clear tidal trend during both seasons, with highest values measured at low tide

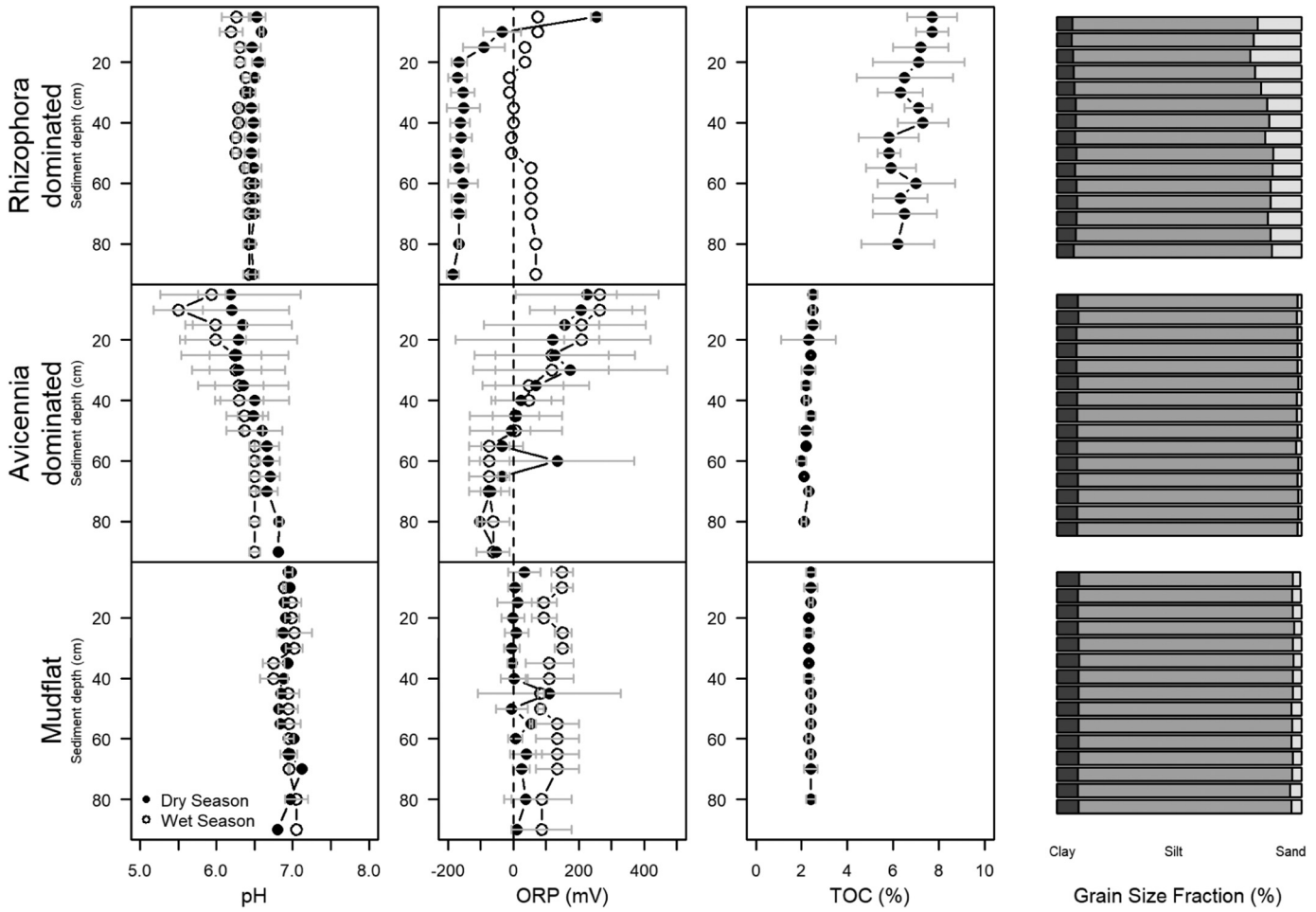


**Fig. 3.** Median value and standard deviation ($n = 3$) of pH, oxidation-reduction potential (ORP in mV), total organic carbon (TOC in %) and grain size fraction (%) in the three land cover stands (*Rhizophora*-dominated, *Avicennia*-dominated, mudflat) along depth, from surface to 100 cm.

and lowest values at high tide (Fig. 5). However, peak values were not observed during the tidal cycle with an amplitude < 1.5 m (i.e. during the second low tide of the "Dry season asymmetric tide" and during the first low tide of the "Wet season asymmetric tide"; c.f. Fig. 5). N-$NO_2^-$, N-$NO_3^-$, and P-$PO_4^{3-}$ concentrations did not follow such a clear tidal pattern (Fig. 5).

Ammonium was the most variable dissolved inorganic nutrient in the creek with concentrations as high as 50.7 µM during the low tide peak, but consistently returning close to 0 µM at high tide (Fig. 5). The N-$NH_4^+$ median value was 2.6 µM. Across a complete diel tidal cycle (24-h) nitrate was the most abundant dissolved inorganic nutrient in the creek water with a median concentration of 9.3 µM, ranging from 0.1 µM to 21.4 µM. Nitrite was almost always below detection range with a median concentration of 0 µM and values up to 5.7 µM.

Greater P-$PO_4^{3-}$ concentrations were measured during the wet season in the tidal creek (Fig. 5). The median P-$PO_4^{3-}$ concentration of 3.1 µM [2.7; 4.3] for the wet season in the creek water was about three-fold higher than during the dry season (1.1 µM [0.4; 1.6]), similar to what was measured for porewater (see 3.1 and Fig. 4).

Nitrogen was again the limiting nutrient most of the time, as suggested by the median DIN:DIP ratio of 7.0 [0.0; 35.3] (Table 1). Still, assimilable nutrients appeared more balanced during the dry season, when P-$PO_4^{3-}$ concentrations were lower. The median DIN:DIP ratio during the dry season was 17.7:1, which is very close to the balanced state even though it was also highly variable throughout time-series with values oscillating from 0:1 to 35.3:1. Overall, the tidal creek water column was a nutrient sink as its corresponding N* value was predominantly < 0 (median = −14.17 [−54.4; 9.35]). This nutrient uptake was overall greater during the wet (N* = −36.5 [−54.4; −18.24]) than the dry season (N* = −4.2 [−14.4; 9.35]), and during the ebb (N* = −34.4 [−41.8; 7.2]) and flood tide (N* = −32.7 [−42.9; 4.6]) rather than during the low (N* = −7.5 [−42.5; 2.8]) and high tide (N* = −8.8 [−54.4; 9.3]).

The nitrate nitrogen stable isotope compositions ($\delta^{15}N_{NO3}$) did not show any clear tidal or seasonal trend, with values ranging from 3.5 to 10.0‰ (Fig. 5). However, significant differences were measured for $\delta^{18}O_{NO3}$ between high and low tides ($W_{2,26} = 150$; $p < .05$), and between seasons ($W_{2,45} = 125$; $p < .005$). Lower $\delta^{18}O_{NO3}$ values were measured during high tide (2.11 ± 1.7‰) compared to low tide (3.52 ± 3.88‰), as well as during the dry season (1.5 ± 2.1‰) versus the wet season (3.3 ± 3.3‰).

In Table 2, we compared the values measured in our samples with those calculated using the $\delta^{18}O_{O2}$ from the atmosphere (23.5 ± 0.3‰; (Kroopnick and Craig, 1972)) and the locally measured $\delta^{18}O_{H2O}$. Based on this estimation, it appeared that nitrate in the tidal creek water column was primarily a product of nitrification during the low and ebb tide periods as the measured $\delta^{18}O_{NO3}$ was contributing > 44% of the predicted $\delta^{18}O_{NO3}$ (Table 2). This calculation suggests that nitrification was also occurring during the high and flood period but that other mechanisms were also adding nitrate as the corresponding measured/calculated ratio was only 29% and 23%, respectively.

### 3.3. End member characteristics

The salinity and pH values showed that the upstream site was clearly dominated by a freshwater input (i.e. Dong Nai River) while the

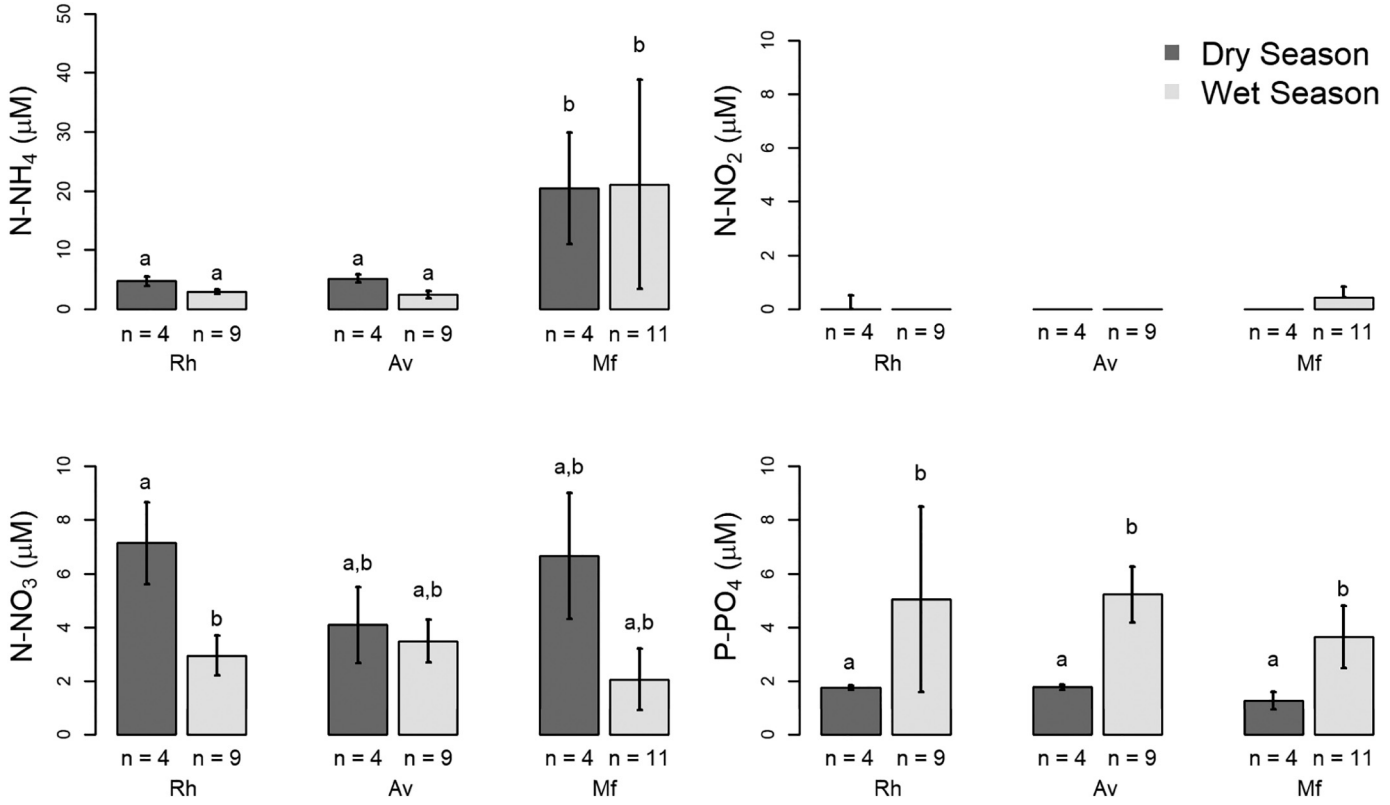


**Fig. 4.** Spatial distribution of the dissolved inorganic nutrients along the ecotone gradient during the dry (dark gray) and wet season (light gray). Rh is for *Rhizophora*-dominated ecotone, Av is for the *Avicennia*-dominated ecotone, and Mf for the mudflat. The statistical significance of the variations between seasons and ecotones was tested using the multiple comparisons non-parametric Kruskal-Wallis rank sum test, and significant differences were highlighted using pairwise Wilcoxon comparisons. Values in each bar plot with different letters (a, b) are statistically different.

downstream site had values representative of a coastal end-member with a maximum salinity of 25.5 (Table 3). There were no significant differences between dissolved inorganic concentrations upstream and downstream the Can Gio mangrove, expect for N-$NO_3^-$ ($W_{2,25} = 123.5$ $p < .01$), where values were much higher upstream (32.8 µM [24.3; 71.4]) than downstream (8.6 µM [5.6; 16.4]) (Table 3). For the two sites, the median DIN:DIP ratio was always < 16:1 indicating that nitrogen was the limiting nutrient (Table 3). $\delta^{13}C$ were significantly more depleted ($W_{2,25} = 259.5$ $p < .001$) upstream (−26.4‰ [−26.8; −26.4]) than downstream (−24.7‰ [−25.0; −24.7]) while $\delta^{15}N$, $\delta^{15}N_{NO3}$ were significantly more enriched ($W_{2,25} = 91$ $p < .001$ and $W_{2,25} = 136$ $p < .05$, respectively) upstream than downstream the Can Gio mangrove (Table 3). Overall, nitrate stable isotope compositions ranged from 8.1‰ to 9.6‰ for $\delta^{15}N_{NO3}$ and from 1.0‰ to 3.7‰ for $\delta^{18}O_{NO3}$ (Table 3).

## 4. Discussion

### *4.1. Influence of mangrove distribution on sediment and porewater characteristics*

#### *4.1.1. Sediment and porewater characteristics are influenced by mangrove stands and seasonality*

The heterogeneity of mangrove sediment chemistry observed within and between the three stands reflects the influence of vegetation distribution and hydrological factors. The three-fold higher total organic carbon content of the *Rhizophora* stand, compared to the *Avicennia* stand and mudflat (Fig. 3), can be explained by four factors. First, *Rhizophora* spp. are more productive than *Avicennia* spp. within the same climatic and geomorphologic conditions and thus generate more litterfall (Saenger and Snedaker, 1993), that may accumulate in the sediment. *Rhizophora* spp. also feature higher belowground biomass (root systems) within the same environment (Alongi et al., 2000; Alongi et al., 2002). Second, the distance from the *Rhizophora* stand to the tidal creek (Fig. 1), together with their dense above-ground root network type, enhance organic matter trapping as opposed to export (Horstman et al., 2015; Krauss et al., 2003; Mazda et al., 1995; Wolanski et al., 1980). Third, the suboxic to reducing sediment conditions observed in the *Rhizophora* stand despite a greater grain size fraction (Fig. 3) limits the aerobic decomposition of organic matter. Energetically less favorable decomposition processes, such as sulfate reduction, prevail in the *Rhizophora* stand, thereby enhancing organic matter burial (Marchand et al., 2004; McKee et al., 1988). Fourth, the *Avicennia* spp. leaves are known to decompose faster than those of *Rhizophora* spp. because they contain more labile nitrogen compounds (Nordhaus et al., 2017). Thus, aboveground and belowground vegetation productivity, distance from the tidal creek, reducing conditions, and lower litter decomposition rates tend to enhance organic matter burial in the *Rhizophora* stand.

The oxidation-reduction potential (ORP) was highly variable between stands, depths and seasons. The oxidizing first few centimeters of the sediment (> 80 mV), particularly apparent in the vegetated stands (Fig. 3), can be directly attributed to air diffusion from the atmosphere and to crab burrows that aerate the sediment, in opposition to more reducing conditions at depth (Kristensen and Alongi, 2006). The absence of seasonal variability of the ORP values in the *Avicennia* stand (Fig. 3) indicates that this vegetation stand is likely to be influenced by cable roots releasing oxygen via an exudate process (Deborde et al., 2015; Marchand et al., 2004). This oxygen input from roots enhances $O_2$ availability within the sediment and consequently aerobic decomposition of organic matter (Marchand et al., 2006). This higher decomposition process is supported by the lower pH values in the *Avicennia* stand mirroring the ORP depth profile (Fig. 3). The large error

**Table 1**
The median [min; max] values of water quality, particulate organic carbon, dissolved inorganic nutrients and stable isotopes in the tidal creek surface water at different tidal stages (high, ebb, low, flood) and in the mangrove sediment porewater (PW) at different stands (*Rhizophora* (Rh), *Avicennia* (Av), mudflat (Mf)).

| | High tide | Ebb Tide | Low Tide | Flood Tide | PW Rh | PW Av | PW Mf |
|---|---|---|---|---|---|---|---|
| n of samples taken | 14 | 8 | 15 | 12 | 13 | 13 | 14 |
| Salinity | $21.0^{a,b}$ | $20.8^{a,b}$ | $21.1^{a,b}$ | $19.2^{a}$ | $22.4^{c}$ | $26.0^{d}$ | $21.3^{b}$ |
| | [19.3; 21.9] | [18.7; 21.7] | [18.9; 22.5] | [15.8; 22.2] | [20.4; 26.3] | [21.2; 29.2] | [20.1; 23.8] |
| pH | $7.5^{a}$ | $7.1^{a,b}$ | $7.1^{b}$ | $7.1^{b}$ | $6.7^{c}$ | $6.6^{c}$ | $6.7^{c}$ |
| | [7.1; 7.6] | [6.9; 7.6] | [6.7; 7.6] | [6.8; 7.6] | [6.4; 7.1] | [6.0; 6.8] | [5.9; 7.1] |
| DO ($mg\,L^{-1}$) | $5.0^{a}$ | $3.8^{a}$ | $3.4^{a}$ | $3.7^{b}$ | N.A. | N.A. | N.A. |
| | [3.6; 6.6] | [3.0; 5.7] | [1.7; 6.1] | [3.1; 5.6] | | | |
| POC (μM) | $65.4^{a}$ | $74.9^{a,b}$ | $156.1^{b}$ | $97.3^{a,b}$ | N.A. | N.A. | N.A. |
| | [33.7; 463.2] | [38.0; 250.5] | [51.4; 775.8] | [26.3; 244.8] | | | |
| $\delta^{13}C$ (‰) | $-26.5^{a}$ | $-27.0^{a}$ | $-26.8^{a}$ | $-26.9^{a}$ | N.A. | N.A. | N.A. |
| | [−28.1; −25.8] | [−27.3; −26.2] | [−27.7; −26.1] | [−29.1; −26.0] | | | |
| $\delta^{15}N$ (‰) | $2.9^{a}$ | $3.1^{a}$ | $3.5^{a}$ | $1.6^{a}$ | N.A. | N.A. | N.A. |
| | [0.0; 4.9] | [1.2; 6.6] | [−3.9; 7.0] | [−5.3; 4.9] | | | |
| P-$PO_4$ (μM) | $1.5^{a}$ | $2.8^{a,b}$ | $1.2^{a}$ | $3.1^{a,b}$ | $4.2^{b,c}$ | $3.7^{c}$ | $3.3^{b,c}$ |
| | [0.4; 4.3] | [1.0; 3.1] | [0.9; 3.3] | [0.7; 3.8] | [1.5; 34.4] | [1.6; 13.5] | [0.2; 14.9] |
| N-$NH_4$ (μM) | $0.0^{a}$ | $1.9^{a,b}$ | $7.9^{b,c}$ | $2.7^{a,b,c}$ | $3.0^{c,d}$ | $4.3^{c}$ | $21.1^{d}$ |
| | [0.0; 3.8] | [0.0; 3.3] | [0; 50.7] | [0.0; 28.7] | [1.7; 5.3] | [1.0; 6.0] | [0.6; 162.4] |
| N-$NO_2$ (μM) | $0.0^{a}$ | $0.0^{a}$ | $0.0^{a}$ | $0.0^{a}$ | $0.0^{a}$ | $0.0^{a}$ | $0.0^{a}$ |
| | [0.0; 2.1] | [0.0; 1.4] | [0.0; 5.7] | [0.0; 2.1] | [0.0; 2.1] | [0.0; 0.0] | [0.0; 3.8] |
| N-$NO_3$ (μM) | $11.4^{a}$ | $6.8^{a}$ | $8.6^{a}$ | $9.6^{a}$ | $3.6^{b}$ | $3.5^{b}$ | $2.8^{b}$ |
| | [3.6; 20.0] | [4.9; 20.0] | [3.4; 20.0] | [3.8; 21.4] | [0.0; 10.0] | [0.0; 6.6] | [0.0; 10.7] |
| N* | $-8.9^{a}$ | $-34.3^{a}$ | $-7.5^{a}$ | $-32.7^{a}$ | $12.2^{b}$ | $25.9^{b}$ | $18.5^{b}$ |
| | [−54.4; 9.4] | [−41.9; 7.2] | [−42.5; 2.8] | [−42.9; 4.6] | [0.6; 51.8] | [1.5; 134.4] | [0.8; 110.0] |
| DIN:DIP | $11.6^{a,b}$ | $6.7^{a}$ | $16.0^{b}$ | $9.2^{,b}$ | $1.6^{c}$ | $1.3^{c}$ | $9.2^{a,c}$ |
| | [0.0; 32.1] | [2.2; 20.4] | [3.5; 35.3] | [1.2; 25.1] | [0.2; 8.8] | [0.2; 6.7] | [0.1; 48.2] |
| $\delta^{15}N_{NO3}$ (‰) | $8.6^{a}$ | $3.1^{a}$ | $8.3^{a}$ | $1.6^{a}$ | $6.9^{a}$ | $2.6^{a}$ | $5.3^{a}$ |
| | [7.8; 9.6] | [1.2; 6.6] | [6.4; 8.3] | [−5.3; 4.9] | [2.6; 9.1] | [−0.9; 12.7] | [2.7; 9.0] |
| $\delta^{18}O_{NO3}$ (‰) | $2.1^{a}$ | $2.5^{a,b}$ | $3.5^{b}$ | $1.6^{a}$ | $5.4^{a,b,c}$ | $14.5^{c}$ | $12.3^{a,b,c}$ |
| | [−1.4; 3.7] | [0.6; 5,8] | [−1.5; 15.1] | [−3.3; 5.9] | [−3.9; 19.3] | [6.6; 23.9] | [0.6; 26.6] |

Values were determined from measurements made over the four 24-h time series and porewater samples collection. The statistical significance of the variations between tidal cycle stages and porewater in mangrove stands was tested using the multiple comparisons non-parametric Kruskal-Wallis rank sum test, and significant differences were highlighted using pairwise Wilcoxon comparisons. Statistical groups were associated with the following letters a, b, c, and d.

bars for ORP values in the *Avicennia* stands illustrate the higher oxygen values close to roots within the sediment.

To summarize, ORP for the three habitats were all suboxic to reducing (< 80 mV) but: (1) seasonal differences were observed in the sediment beneath the *Rhizophor*a vegetation and in the mudflat; and (2) the 50 first cm in the sediment under the *Avicennia* vegetation were oxic to suboxic (> 0 mV) because of $O_2$ inputs from their root systems. The redox conditions in the sediment are essential for understanding the belowground nutrient dynamics.

#### 4.1.2. Nitrogen dynamics in porewater are influenced by the presence or absence of mangrove vegetation

The much greater N-$NH_4^+$ concentrations in the mudflat, in comparison with the two vegetated stands (Fig. 4), may be explained by N-$NH_4^+$ uptake by vegetation (Alongi, 1996; Deborde et al., 2015; Middelburg et al., 1996). The high N-$NH_4^+$ concentrations in the mudflat stand (21.1 μM [0.5; 162.4]) indicate a high mineralization (ammonification) process. Because no permanent macrophytic vegetation is present in the mudflat to consume the dissolved nutrients, N-$NH_4^+$ accumulates and becomes available for nitrification or discharge via porewater seepage. Interestingly, no significant differences were measured in nitrate concentrations between the three stands ($H_{3,29} = 1.03$; $p = .7949$), N-$NO_3^-$ always remaining below 11 μm, even though N-$NH_4^+$ concentrations were much higher in the mudflat stand. Moderately to strongly reducing conditions of the mangrove sediment (< 80 mV), as described previously, might account for the main nitrification inhibitor.

#### 4.1.3. Phosphorus dynamics in porewater are influenced by seasonality

The higher P-$PO_4^{3-}$ concentrations during the wet season can be explained by the influence of biotic processes. Phosphate in mangrove sediments originates from organic matter decomposition (as particulate organic phosphorus) and root exudates (as dissolved organic phosphorus) (Holmer et al., 1994). The release of P through OM degradation is driven by phosphate-solubilizing bacteria (PSB), which develop predominantly on mangrove roots but can also operate in sediments and the water column (Ray et al., 2017; Reef et al., 2010; Vazquez et al., 2000). Greater phosphate concentrations during the wet season are consistent with the suggested higher ecosystem and bacterial productivity during the same period when rainfall increases and atmospheric temperatures remain within the same range (Behera et al., 2014; Koné and Borges, 2008; Linto et al., 2014; Taillardat et al., 2018b). Frequent and intense rain events reduce porewater salinity and mobilize organic matter, which is likely to increase phosphate solubilization and mineralization.

### 4.2. Nutrients sources and dynamics in a mangrove tidal creek

#### 4.2.1. Seasonal variability of phosphate in the tidal creek

The phosphate concentrations in the creek water had no clear tidal trend but showed distinct ranges between seasons, with values being about three-fold higher during the wet season. This observation is similar to the P-$PO_4^3$ porewater signal we previously described (see 4.1.3). Hence, the biotic factor (enhanced activity of phosphate solubilizing bacteria) previously described for P-$PO_4^3$ seasonal variation in porewaters is likely to also explain the seasonal evolution of the creek water P-$PO_4^3$ concentrations.

The absence of a clear tidal trend may be explained by the contributions of both a slight discharge of mangrove sediments P-$PO_4^3$ via porewater seepage at low tide as previously suggested (Dittmar and Lara, 2001a; Ovalle et al., 1990; Santos et al., 2014) and an import from the river estuarine system during the rising tides, as the estuarine P-$PO_4^3$ concentrations were higher (5.3 ± 1.0 μM; Table 3) than those of the tidal creek (1.6 ± 1.1 μM; Table 1). Unlike most of the regional

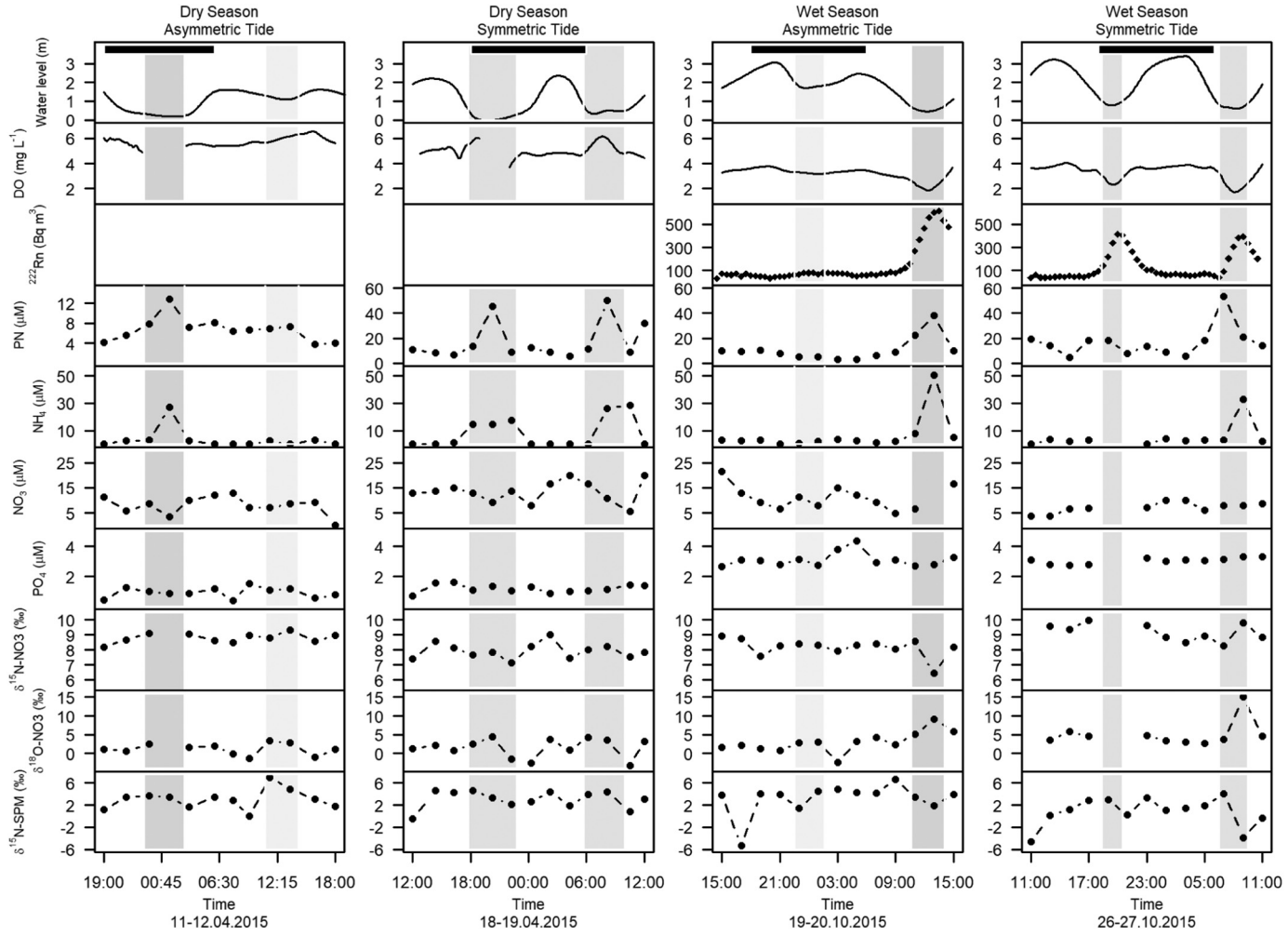


**Fig. 5.** Time series (24-h) of several dissolved parameters, particulate nitrogen (PN), and suspended particulate matter (SPM) in the Can Gio Mangrove tidal creek water surface in April 2015 (dry season asymmetric tide and dry season symmetric tide) and October 2015 (wet season asymmetric tide and wet season symmetric tide). Each Y-axis is consistent for the same variable throughout the four time series. Radon ($^{222}$Rn) was not measured during the dry season due to technical difficulties. The gray background shading indicates the low tide period; the black banner at the top indicates night.

**Table 2**
Comparison of the $\delta^{18}O_{NO3}$ from the measured samples and the theoretically calculated values. Values are presented as the median [min; max].

| | Measured $\delta^{18}O_{H2O}$ | Measured $\delta^{18}O_{NO3}$ | Calculated $\delta^{18}O_{NO3}$ | (Meas./ Calc) |
|---|---|---|---|---|
| | (‰) | (‰) | (‰) | |
| *Tidal stages* | | | | |
| Low Tide | −2.83 [−3.00; −2.60] | 3.49 [01.49; 15.13] | 5.95 [5.83; 6.10] | 59% |
| High Tide | −2.80 [−2.87; −2.63] | 2.08 [−1.4; 3.66] | 5.97 [5.92; 6.08] | 29% |
| Ebb Tide | −2.80 [−2.96; −2.57] | 2.46 [0.63; 5.84] | 5.87 [5.86; 6.12] | 45% |
| Flood Tide | −2.95 [−3.68; −2.73] | 1.60 [−3.3; 5.87] | 5.87 [5.38; 6.02] | 23% |

When nitrification occurs, the measured value is supposed to be close the to calculated value, which combines 2/3 $\delta^{18}O_{H2O}$ (column 1) and 1/3 $\delta^{18}O_{air}$ (Kendall et al., 2007; Kroopnick and Craig, 1972).

mangrove systems that are P-limiting (Holmer et al., 2001; Kristensen and Suraswadi, 2002; Trott and Alongi, 1999), the use of the Redfield DIN:DIP referential ratio of 16:1 (Redfield, 1958) suggests DIN ($NH_4^+$ + $NO_2^-$ + $NO_3^-$) to be the limiting element most of the time (median DIN:DIP = 7.0:1; range 0:1–35.3:1), and particularly during the wet season (DIN:DIP = 4.0:1 [1.2:1; 19.0]). However, the episodic release of N-$NH_4^+$ through porewater seepage during ebb tide moved the DIN:DIP ratio above 16:1, thus, possibly inducing phytoplankton bloom as observed by David et al. (2018) during the wet asymmetric tide (Fig. 5) presented in this study. Although our study focuses on dissolved inorganic nutrients as they account for the preferential form consumed by primary producers, some studies have shown that dissolved organic nutrients could be assimilated, particularly in nutrient-limited conditions (Glibert et al., 2004; Vonk et al., 2008). Dissolved organic nitrogen and dissolved organic phosphorus concentrations are within the same order of magnitude of the dissolved inorganic fraction in undisturbed mangrove tidal creeks (Dittmar and Lara, 2001b; Gleeson et al., 2013; Tait et al., 2017), and of lower importance in sites with upstream activities generating nutrients input (Wang et al., 2019). Therefore, it is possible that organic nutrients also contribute, to some extent, to the aquatic productivity in mangroves before mineralization. Their contribution will require further investigation to estimate the importance of this pathway.

**Table 3**
River Upstream and Estuary Downstream end-members median [min; max] characteristics.

| | River Upstream | Estuary Downstream |
|---|---|---|
| n | 3 | 3 |
| Salinity | 0.2*** | 25.5*** |
| | [0.2; 0.5] | [24.1; 25.6] |
| pH | 6.6*** | 7.7*** |
| | [6.5; 6.6] | [7.6; 7.7] |
| DO | 1.3*** | 5.2*** |
| ($mg\,L^{-1}$) | [1.1; 1;7] | [4.7; 5.2] |
| POC | 272 | 293 |
| (μM) | [245.4; 455.9] | [240.7; 443.8] |
| $\delta^{13}C$ | −26.4*** | −24.7*** |
| (‰) | [−26.8; −26.4] | [−25.0; −24.7] |
| $\delta^{15}N$ | 7.9*** | 5.4*** |
| (‰) | [7.9; 8.6] | [5.1; 5.5] |
| $P\text{-}PO_4$ | 7.8 | 5.3 |
| (μM) | [4.0; 7.9] | [4.0; 6.0] |
| $N\text{-}NH_4$ | 2.0 | 0 |
| (μM) | [1.2; 5.6] | [0; 5.2] |
| $N\text{-}NO_2$ | 0.0 | 0.0 |
| (μM) | [0.0; 1.4] | [0.0; 3.6] |
| $N\text{-}NO_3$ | 32.8** | 8.6** |
| (μM) | [24.3; 71.4] | [5.6; 16.4] |
| N* | −115.5 | −76.2 |
| | [−116.8; −54.0] | [−86.7; −55.2] |
| DIN:DIP | 5.1 | 2.0 |
| | [3.4; 18.1] | [1.4; 4.0] |
| $\delta^{15}N_{NO3}$ | 9.5* | 8.2* |
| (‰) | [9.1; 9.6] | [8.1; 9.0] |
| $\delta^{18}O_{NO3}$ | 2.1* | 2.4* |
| (‰) | [1.0; 3.3] | [1.7; 3.7] |

The statistical significance of the variations between the two study sites was tested for each variable presented in the table using the following Wilcoxon (W) non-parametric tests. Statistical levels were associated with the following *p*-values < .05*; < 0.01**, and < 0.001***.

#### 4.2.2. Ammonium porewater discharge during the low tide period

Ammonium concentration peaks at low tide were coupled to high $^{222}Rn$ values. This suggests that porewater discharge was the main source of ammonium in the tidal creek during both dry and wet seasons (Fig. 5 and Table 1). The other forms of dissolved inorganic nitrogen ($N\text{-}NO_2^-$, $N\text{-}NO_3^-$) and phosphorus ($P\text{-}PO_4^{3-}$) did not seem to originate from the mangrove porewater directly or predominantly as no tidal trends existed (Fig. 5), nor was there a correlation with $^{222}Rn$. Prior studies assessing nutrient dynamics in other mangrove tidal creeks reported similar patterns (i.e. discharge of $N\text{-}NH_4^+$), with the only difference being that $P\text{-}PO_4^{3-}$ porewater discharge was sometimes measured (Dittmar, 1999; Gleeson et al., 2013; Maher et al., 2016; Ovalle et al., 1990; Tait et al., 2017; Wang et al., 2019). The tidal creek $N\text{-}NH_4^+$ concentrations at low tide (7.9 μM [0; 50.7]) were significantly lower than the porewater concentrations at the mudflat stand (21.1 μM [0.5; 162.4]) and not significantly higher than those of the two vegetation stands (3.0 μM [1.7; 5.3] for *Rhizophora*; 4.3 μM [1.0; 6.0] for *Avicennia*) (Table 1). Thus, the $N\text{-}NH_4^+$ mangrove porewater discharge was dominated by a discharge from the mudflat. This important finding suggests that vegetation uptake makes the mangrove vegetated area a sink of $N\text{-}NH_4^+$, while the unvegetated mudflat is a source of $N\text{-}NH_4^+$, because of high N mineralization (ammonification), limited uptake (as suggested by N* > 0) and porewater discharge (lateral export of $N\text{-}NH_4^+$). This also suggests that most of the porewater discharge occurs at a short distance from the creek bank. Further investigations are needed as this could also be the case for carbon porewater discharge.

#### 4.2.3. Nitrate input from in situ nitrification and from the river-estuarine system

Based on the measured $\delta^{18}O_{NO3}$ versus calculated $\delta^{18}O_{NO3}$ described earlier, it appears that nitrification was a dominant source of nitrate in the tidal creek, particularly during the low and ebb periods, when the measured $\delta^{18}O_{NO3}$/calculated $\delta^{18}O_{NO3}$ ratios were 59% and 41%,

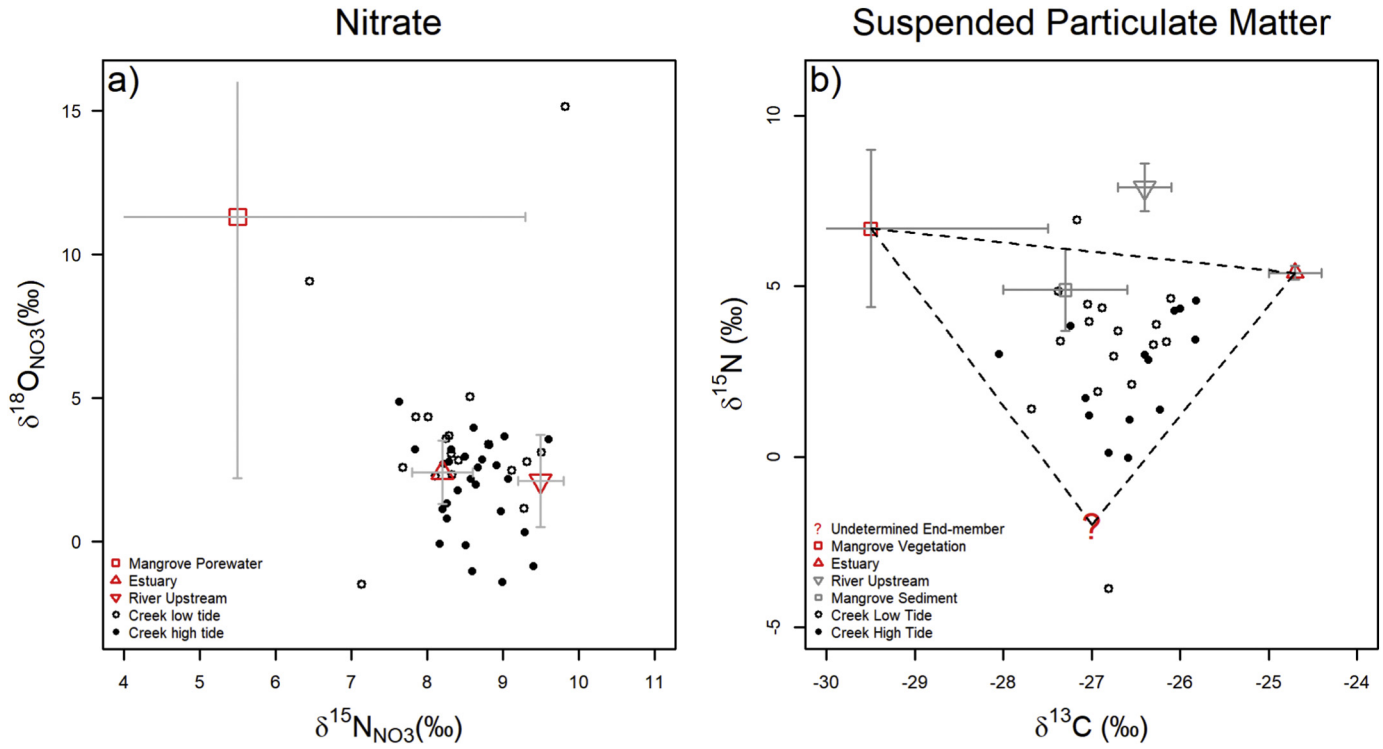


**Fig. 6.** (a) $\delta^{15}N_{NO3}$ and $\delta^{18}O_{NO3}$ in the mangrove tidal creek water surface during the low (empty circles) and high (black bullets) tide periods. End-members are indicated in red with gray error bars. (b) $\delta^{13}C$ and $\delta^{15}N$ of the mangrove tidal creek suspended particulate matter during the low (empty circles) and high (black bullets) tide periods. End-members are indicated in red or gray with gray error bars. The question mark represents the undetermined end-member fixed at $\delta^{13}C$ of −27‰ and $\delta^{15}N$ of −2‰, based on the distribution of the suspended particulate matter isotope compositions.

respectively (Table 2). We explain this nitrification process as a result of $N\text{-}NH_4^+$ from porewater discharge in contact with higher oxygen concentrations in the tidal creek and with the atmosphere (Gleeson et al., 2013). The contribution of in situ nitrification was, however, calculated to be lower during flood (27%) and high tides (35%) (Table 2). It is possible that in the dynamic tidally-influenced creek system, other allochthonous sources bring nitrate during these tides — this can be tested via the study of the nitrate dual stable isotope compositions.

Plotting the two nitrate isotope compositions ($\delta^{15}N_{NO3}$ & $\delta^{18}O_{NO3}$) provides information on sources and transformation processes (Kendall et al., 2007). Based on the theoretical values developed by Kendall et al. (2007), all the tidal creek surface water samples were plotted in an area that corresponds to nitrate from soil ammonium nitrification, nitrate from manure and sewage as well as marine nitrate. Among those samples, we were able to clearly separate the low tide samples from the high tide samples (Fig. 6a). While most of the samples at high tide were clustered close to the river upstream and estuary end-member values, the low tide samples leaned towards the nitrate mangrove porewater end-member (Fig. 6a). Therefore, our data suggests that nitrate may come from two distinct sources in the mangrove tidal creek: (1) nitrified porewater-derived ammonium during ebb and low tide; and (2) river-derived nitrate during flood and high tide.

Nitrate dual stable isotopes can also provide relevant information to estimate denitrification. If denitrification were to happen, then the relation between the two stable isotopes would result in a slope coefficient between 1 and 2 (Kendall et al., 2007) which was not observed here (Fig. 6a). Plotting $\delta^{15}N_{NO3}$ against $NO_3^-$ concentrations, $\ln(NO_3^-)$ and $1/NO_3^-$ can also reveal denitrification rate (Archana et al., 2018; Wankel et al., 2009) but not from our dataset (not shown). However, while we observed no clear trend that would unambiguously identify denitrification as a key process in our study, this does not necessarily mean that it did not occur. Using the same approach along with $N_2O$ measurements and sediment molecular gene analysis, a recent study conducted in a human-impacted mangrove in Southeast China identified denitrification as a major process in the mangrove N cycle (Wang et al., 2019). Another study in a disturbed mangrove tidal creek of Southeast China also reported denitrification (Xiao et al., 2018). The authors hypothesized a higher denitrifying microbial activity in these locations rather than in reducing deep porewater because of a higher organic matter and nutrients availability coupled to lower salinization. Still, limited denitrification as our results suggest is consistent with the estimates from Alongi (2013). The author accounted denitrification for < 5% of the total nitrate output in mangrove environments since it is considered as an inefficient pathway in oligotrophic conditions generating a net loss of N from the system through $N_2O$ emissions (Alongi, 2018; Maher et al., 2016). Thus, even though denitrification may have occurred in our study site, it most probably remained a minor pathway of nitrogen loss from the system.

#### 4.2.4. Particulate nitrogen in the tidal creek: The contribution of the mangrove vegetation and estuarine organic matter

In addition to the $N\text{-}NH_4^+$ discharge via porewater seepage, surface runoff and creek bottom sediment re-suspension also contributed to the N input from the mangrove to the tidal creek. Highest concentrations of particulate nitrogen (53.47 μM) were measured during the lowest low tides (e.g. Time series #4 in Fig. 5). The peak was proportional to the suspended particulate matter concentrations, which increased at the end of the ebb tide because of surface sediment runoff and sediment re-suspension (Bouillon et al., 2007; Kristensen and Suraswadi, 2002). Thus, the particulate nitrogen at low tide in the tidal creek appears to predominantly originate from the mangrove vegetation and sediments (Fig. 6b). This contribution was, however, not constant throughout complete tidal cycles as other sources appeared to influence the tidal creek particulate and dissolved nitrogen dynamics.

The origin of suspended particulate matter (SPM) in the tidal creek was investigated using $\delta^{13}C$ and $\delta^{15}N$ (Fig. 6b). Alone, the $\delta^{13}C$ values of the mangrove vegetation and estuarine end-members are able to explain the variability and the origin of the tidal creek SPM, as all the creek water samples were within the values measured for these two end members ($-28.4 \pm 1.3$‰ for the mangrove vegetation; $-24.7 \pm 0.2$‰ for the estuary) (Fig. 6b). However, the $\delta^{15}N$-SPM measured in the tidal creek had more depleted values ($-5.3$ to 6.7‰) than the $\delta^{15}N$ of the mangrove vegetation end-member (6.9 ± 2.7‰) and the estuarine SPM end-member (5.4 ± 0.2‰) (Fig. 6). This was particularly evident during high tide, suggesting that another end-member or transformation process was decreasing the $\delta^{15}N$-SPM at this moment (Fig. 6b).

Autotrophic (phytoplankton, microphytobenthos, and macroalgae) and/or heterotrophic (bacteria, protozoa, and zooplankton) organisms may have contributed to the pool of particulate organic nitrogen (PON) during a particular phase of the tidal cycle. A previous study conducted in the same tidal creek during the same period demonstrated that phytoplankton proliferates during rising tides by consuming porewater-derived nutrients and $CO_2$ (David et al., 2018). Considering the $\delta^{15}N$ value near 0‰, an atmospheric $N_2$-fixing organism may be considered. In coastal waters, only cyanobacteria (either free-living or developed on symbionts with diatoms) are able to assimilate atmospheric $N_2$ (Zehr and Kudela, 2011). Production of $N_2$ in the Amazon mouth via cyanobacteria was reported with water conditions comparable to mangrove tidal creek hydrodynamics (e.g. low water velocity in comparison to estuaries, light-limiting conditions, trace metals available through porewater discharge) (Subramaniam et al., 2008). Organisms fixing $N_2$ are also most probably growing on sediment surface and/or mangrove roots at this site as exceptionally low $\delta^{15}N$ values (1.1 ± 0.7‰) were observed in the tissues of a gastropod feeding by scrapping the mangrove roots (David et al., 2019). Such microorganisms could possibly be resuspended at high tide.

Upstream inputs of agricultural fertilizers could also have constituted the missing end member, with $\delta^{15}N$ values generally near 0‰ (Finlay and Kendall, 2007). However, agricultural lands are located upstream the River sampling site which had a value of 7.9‰ (Table 3). Therefore, it is not possible to consider agricultural fertilizer as a source of nutrients in the tidal creek if this source did not affect the river site located in between the two locations. While we cannot confirm the origin of the missing end-member, our dataset along with the findings from David et al. (2019) suggest that $N_2$-fixing organisms are present in this ecosystem and that their contribution to the water column PON pool is significant. Measurements such as quantitative metabarcoding would provide more insights into the identification of such organisms.

Therefore, we suggest that the particulate nitrogen in the mangrove tidal creek mainly originates from: (1) the mangrove vegetation at low tide, (2) estuarine waters at high tide, and (3) phytoplanktonic activity having consumed porewater-derived ammonium and $CO_2$ during rising tides. In addition, $N_2$-fixing organisms probably contribute to the PON pool, but their dynamics and their identification would require further investigations.

### 4.3. Implications for the mangrove outwelling hypothesis

The results of this study and other studies recently conducted by our team in the same tidal creek (David et al., 2018; David et al., 2019; Taillardat et al., 2018a; Taillardat et al., 2018b) provide new insights into mangrove biogeochemical cycling and identified research gaps in relation to the Outwelling Hypothesis. The biggest challenge related to the Outwelling Hypothesis has always been to understand how mangrove-derived organic matter, with low nutritive value and high tannins content, could indeed represent a primary and significant food resource for aquatic consumers (Lee, 1995). The present study suggests that nutrients are released from the mangrove forest mainly in their inorganic form, as a result of belowground mineralization, rather than through litter and macroelements export. Although the importance of

mineralization has been proposed since the early development of the hypothesis (Odum and Heald, 1975), this transformation process was originally only expected on sediment surface or in the water column. Porewater discharge was suggested as a key mechanism in the Outwelling process but remains largely underappreciated (Lee, 1995). Previous studies also revealed high concentrations of dissolved inorganic carbon including dissolved $CO_2$ being released via porewater discharge (Call et al., 2015; Call et al., 2019b; Maher et al., 2013; Taillardat et al., 2018b). Dissolved inorganic nutrients, including $CO_2$ and $N\text{-}NH_4^+$ are required for autotrophic organisms such as phytoplankton. The identification of mangrove porewater discharge (Fig. 5), along with particulate C and N stable isotope compositions and nitrate dual stable isotope compositions (Fig. 6) all suggest that mangrove mineralized material is rapidly consumed and may sustain aquatic primary production.

The role of phytoplankton as a transporter of nutrients has also been suggested but, as our study revealed, stable isotope makes the quantification of its contribution challenging (Bouillon et al., 2008; Fry and Smith, 2002). However, the use of fatty acids (David et al., 2019) and the construction of time series measurements, able to capture short duration events such as phytoplankton blooms (David et al., 2018) have proven to be useful for supporting the argument that phytoplankton is part of the mangrove coastal food web and grows on mangrove-derived inorganic nutrients (Fig. 7).

Another challenge to the hypothesis was the limited spatial extent of the mangrove Outwelling (Claudino et al., 2015; Lee, 1995). Our results demonstrate that mangrove-derived ammonium is rapidly consumed within the tidal creek, most probably by phytoplankton. Consequently, we propose that mangrove-derived inorganic nutrients support the primary link of the coastal food web, which is later assimilated by other organisms within the trophic chain, up to mobile macroconsumers such as fishes and shrimps (David et al., 2019). The role of mangroves as nurseries is another ecological theory lacking clear and consistent evidence (Lee et al., 2014) but macroconsumers migration in and out mangroves has been observed (Claudino et al., 2015). Considering that phytoplankton is highly nutritive, it is realistic to consider organisms of the higher trophic level to eat and develop in the mangrove environment and then eventually migrate towards coastal waters where they will release subsidies and serve as food for other organisms. Thus, the macroconsumers migration could be considered as the ultimate mangrove-derived nutrients Outwelling (Fig. 7).

## 5. Conclusions

Nutrient concentrations and forms in mangrove ecosystems are spatially and temporally variable. The use of organic matter and nitrate stable isotopes, along with dissolved inorganic nutrient concentrations have helped to constrain nitrogen and phosphorus dynamics in mangrove sediments and tidal creeks. Our study showed that ammonium was the dominant form of dissolved inorganic nitrogen in the sediment porewater. Litterfall and root exudates released dissolved organic matter that was mineralized by soil bacteria, producing inorganic nutrients such as ammonium and phosphate. However, a fraction of these recycled nutrients was directly taken up by mangrove vegetation. Consequently, dissolved inorganic concentrations were greater at the mudflat stand, located on the edge of the tidal creek, as no vegetation was taking up the available nutrients. During low tide, ammonium was released to the tidal creek from the mudflat via porewater discharge. Thus, our study showed that mangrove sediments were a place where nutrient recycling, uptake, and discharge occurred.

Concentrations and origins of dissolved inorganic nutrients in the tidal creek were also disparate. Using stable isotopes, we identified a clear contribution from mangrove organic matter and mangrove porewater during the low tide period. During the flooding and high tide periods, our result suggested that input from the river-estuarine system was the dominant output with concentrations similar to what was measured during the low tide period, except for ammonium. Thus, a straightforward nutrient Outwelling from the mangrove to the coastal waters was not evident in our study site. Still, the compilation of different studies conducted within this same tidal creek made us reconsider the mangrove Outwelling hypothesis. We propose that the coastal nutrient exchange occurs in the mangrove tidal creek where ammonium is being discharged from porewater, nitrified, and utilized by phytoplankton later consumed by aquatic macro-organisms. These mobile organisms such as shrimps and fishes are then moving towards coastal waters where they will themselves feed other organisms. This

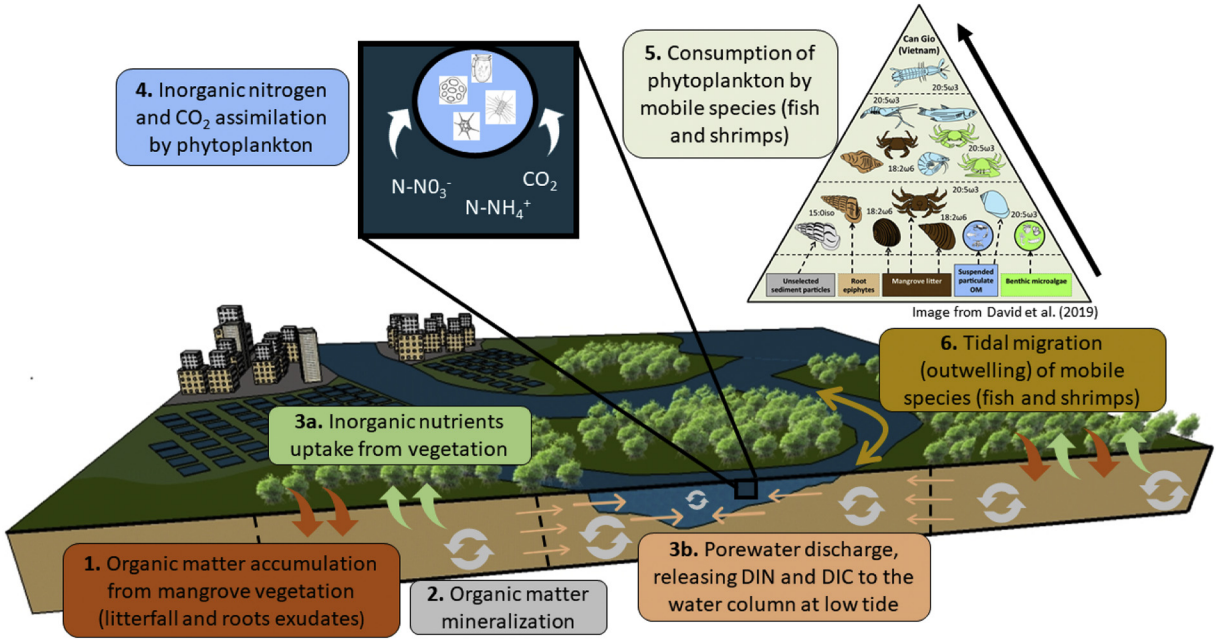


**Fig. 7.** Conceptual model of the mangrove-derived organic matter nutrients dynamics in the Can Gio mangrove ecosystem. This interpretation is based on this study along with other publications conducted within the same mangrove tidal creek (David et al., 2018; David et al., 2019; Taillardat et al., 2018a; Taillardat et al., 2018b).

scenario can be seen as a form of a mangrove Outwelling. Consequently, this study provides additional evidence that mangroves are highly efficient systems in a nutrient-depleted environment depending on internal reuse of resources to support ecosystem productivity, with a tight connection and biogeochemical complementarity between vegetation, micro and macro-organisms.

## Acknowledgements

The authors thank students from Nong Lam University, University of Science Vietnam National University for assistance in the field, Émilie Strady (Institut de Recherche pour le Développement) for laboratory space, Agniezska Adamowicz-Walczak and Jean François Hélie (Université du Québec à Montréal) for assistance and advice related to laboratory work, Ana Maria Escobar Cardenas for 3D graphical work. This project was supported by the Singapore Academic Research Fund [R-109-000-192-112], the NUS Graduate Research Support Scheme, the Fonds de Recherche du Québec – Nature et Technologies (FRQNT), and the Air Liquide Foundation.

## Declarations of interest

None.

## References

Adame, M.F., Lovelock, C.E., 2011. Carbon and nutrient exchange of mangrove forests with the coastal ocean. Hydrobiologia 663, 23–50.
Adame, M.F., Virdis, B., Lovelock, C.E., 2010. Effect of geomorphological setting and rainfall on nutrient exchange in mangroves during tidal inundation. Mar. Freshw. Res. 61, 1197–1206.
Alongi, D.M., 1996. The dynamics of benthic nutrient pools and fluxes in tropical mangrove forests. J. Mar. Res. 54, 123–148.
Alongi, D., 2009. The Energetics of Mangrove Forests. Springer.
Alongi, D.M., 2013. Cycling and global fluxes of nitrogen in mangroves. Glob. Environ. Res. 17, 173–182.
Alongi, D., 2018. Impact of global change on nutrient dynamics in mangrove forests. Forests 9, 596.
Alongi, D., Tirendi, F., Clough, B., 2000. Below-ground decomposition of organic matter in forests of the mangroves Rhizophora stylosa and Avicennia marina along the arid coast of Western Australia. Aquat. Bot. 68, 97–122.
Alongi, D., Trott, L., Wattayakorn, G., Clough, B., 2002. Below-ground nitrogen cycling in relation to net canopy production in mangrove forests of southern Thailand. Mar. Biol. 140, 855–864.
Archana, A., Thibodeau, B., Geeraert, N., Xu, M.N., Kao, S.-J., Baker, D.M., 2018. Nitrogen sources and cycling revealed by dual isotopes of nitrate in a complex urbanized environment. Water Res. 142, 459–470.
Arnaud-Haond, S., Duarte, C.M., Teixeira, S., Massa, S.I., Terrados, J., Tri, N.H., Hong, P.N., Serrão, E.A., 2009. Genetic recolonization of mangrove: genetic diversity still increasing in the Mekong Delta 30 years after Agent Orange. Mar. Ecol. Prog. Ser. 390, 129–135.
Behera, B., Singdevsachan, S., Mishra, R., Dutta, S., Thatoi, H., 2014. Diversity, mechanism and biotechnology of phosphate solubilising microorganism in mangrove—a review. Biocatal. Agric. Biotechnol. 3, 97–110.
Boto, K.G., Bunt, J.S., 1981. Tidal export of particulate organic matter from a northern Australian mangrove system. Estuar. Coast. Shelf Sci. 13, 247–255.
Bouillon, S., Middelburg, J.J., Dehairs, F., Borges, A.V., Abril, G., Flindt, M.R., Ulomi, S., Kristensen, E., 2007. Importance of intertidal sediment processes and porewater exchange on the water column biogeochemistry in a pristine mangrove creek (Ras Dege, Tanzania). Biogeosciences 4, 311–322.
Bouillon, S., Connolly, R.M., Lee, S.Y., 2008. Organic matter exchange and cycling in mangrove ecosystems: recent insights from stable isotope studies. J. Sea Res. 59, 44–58.
Bouillon, S., Connolly, R., Gillikin, D., 2011. 07 Use of Stable Isotopes to Understand Food Webs and Ecosystem Functioning in Estuaries. vol. 7.
Brand, W.A., Coplen, T.B., Vogl, J., Rosner, M., Prohaska, T., 2014. Assessment of international reference materials for isotope-ratio analysis (IUPAC Technical Report). Pure Appl. Chem. 86, 425–467.
Burnett, W., Kim, G., Lane-Smith, D., 2001. A continuous monitor for assessment of 222Rn in the coastal ocean. J. Radioanal. Nucl. Chem. 249, 167–172.
Call, M., Maher, D., Santos, I., Ruiz-Halpern, S., Mangion, P., Sanders, C., Erler, D., Oakes, J., Rosentreter, J., Murray, R., 2015. Spatial and temporal variability of carbon dioxide and methane fluxes over semi-diurnal and spring–neap–spring timescales in a mangrove creek. Geochim. Cosmochim. Acta 150, 211–225.
Call, M., Sanders, C.J., Macklin, P.A., Santos, I.R., Maher, D.T., 2019a. Carbon outwelling and emissions from two contrasting mangrove creeks during the monsoon storm season in Palau, Micronesia. Estuar. Coast. Shelf Sci. 218, 340–348.
Call, M., Santos, I.R., Dittmar, T., de Rezende, C.E., Asp, N.E., Maher, D.T., 2019b. High pore-water derived CO2 and CH4 emissions from a macro-tidal mangrove creek in the Amazon region. Geochim. Cosmochim. Acta 247, 106–120.
Claudino, M.C., Pessanha, A.L.M., Araújo, F.G., Garcia, A.M., 2015. Trophic connectivity and basal food sources sustaining tropical aquatic consumers along a mangrove to ocean gradient. Estuar. Coast. Shelf Sci. 167, 45–55.
Conley, D.C., 2015. Drivers: Waves and Tides, Coastal Environments and Global Change. John Wiley & Sons, Ltd, pp. 79–103.
Coplen, T.B., 2011. Guidelines and recommended terms for expression of stable-isotope-ratio and gas-ratio measurement results. Rapid Commun. Mass Spectrom. 25, 2538–2560.
David, F., Marchand, C., Taillardat, P., Thành-Nho, N., Meziane, T., 2018. Nutritional composition of suspended particulate matter in a tropical mangrove creek during a tidal cycle (Can Gio, Vietnam). Estuar. Coast. Shelf Sci. 200, 126–130.
David, F., Marchand, C., Thành-Nho, N., Truong Van, V., Taillardat, P., Meziane, T., 2019. Trophic relationships and basal resource utilisation in the Can Gio Mangrove Biosphere Reserve (Southern Vietnam). J. Sea Res. 145, 35–43.
Deborde, J., Marchand, C., Molnar, N., Patrona, L.D., Meziane, T., 2015. Concentrations and fractionation of carbon, iron, sulfur, nitrogen and phosphorus in mangrove sediments along an intertidal gradient (semi-arid climate, New Caledonia). J. Mar. Sci. Eng. 3, 52–72.
Dittmar, T., 1999. Nutrient dynamics in a mangrove creek (North Brazil) during the dry season. Mangrove Salt Marshes 3, 185–195.
Dittmar, T., Lara, R.J., 2001a. Driving forces behind nutrient and organic matter dynamics in a mangrove tidal creek in North Brazil. Estuar. Coast. Shelf Sci. 52, 249–259.
Dittmar, T., Lara, R.J., 2001b. Do mangroves rather than rivers provide nutrients to coastal environments south of the Amazon River? Evidence from long-term flux measurements. Mar. Ecol. Prog. Ser. 213, 67–77.
Dittmar, T., Hertkorn, N., Kattner, G., Lara, R.J., 2006. Mangroves, a major source of dissolved organic carbon to the oceans. Glob. Biogeochem. Cycles 20.
Dung, L.V., Tue, N.T., Nhuan, M.T., Omori, K., 2016. Carbon storage in a restored mangrove forest in Can Gio Mangrove Forest Park, Mekong Delta, Vietnam. For. Ecol. Manag. 380, 31–40.
Feller, I.C., Whigham, D.F., McKee, K.L., Lovelock, C.E., 2003. Nitrogen limitation of growth and nutrient dynamics in a disturbed mangrove forest, Indian River Lagoon, Florida. Oecologia 134, 405–414.
Finlay, J.C., Kendall, C., 2007. Stable isotope tracing of temporal and spatial variability in organic matter sources to freshwater ecosystems. Stable Isotopes Ecol. Environ. Sci. 2, 283–333.
Fry, B., Smith, T.J., 2002. Stable isotope studies of red mangroves and filter feeders from the Shark River estuary, Florida. Bull. Mar. Sci. 70, 871–890.
Gleeson, J., Santos, I.R., Maher, D.T., Golsby-Smith, L., 2013. Groundwater-surface water exchange in a mangrove tidal creek: evidence from natural geochemical tracers and implications for nutrient budgets. Mar. Chem. 156, 27–37.
Glibert, P., Heil, C.A., Hollander, D., Revilla, M., Hoare, A., Alexander, J., Murasko, S., 2004. Evidence for dissolved organic nitrogen and phosphorus uptake during a cyanobacterial bloom in Florida Bay. Mar. Ecol. Prog. Ser. 280, 73–83.
Grayman, W., Day, H., Luken, R., 2003. Regional water quality management for the Dong Nai River Basin, Vietnam. Water Sci. Technol. 48, 17–23.
Gruber, N., Sarmiento, J.L., 1997. Global patterns of marine nitrogen fixation and denitrification. Glob. Biogeochem. Cycles 11, 235–266.
Hélie, J., 2009. Elemental and stable isotopic approaches for studying the organic and inorganic carbon components in natural samples, IOP Conference Series: Earth and Environmental Science. IOP Publishing, pp. 012005.
Holmer, M., Kristensen, E., Banta, G., Hansen, K., Jensen, M.H., Bussawarit, N., 1994. Biogeochemical cycling of sulfur and iron in sediments of a south-east Asian mangrove, Phuket Island, Thailand. Biogeochemistry 26, 145–161.
Holmer, M., Andersen, F.O., Nielsen, S.L., Boschker, H.T.S., 2001. The importance of mineralization based on sulfate reduction for nutrient regeneration in tropical seagrass sediments. Aquat. Bot. 71, 1–17.
Horstman, E.M., Dohmen-Janssen, C.M., Bouma, T.J., Hulscher, S., 2015. Tidal-scale flow routing and sedimentation in mangrove forests: combining field data and numerical modelling. Geomorphology 228, 244–262.
Kendall, C., Elliott, E.M., Wankel, S.D., 2007. Tracing anthropogenic inputs of nitrogen to ecosystems. Stable Isotopes Ecol. Environ. Sci. 2, 375–449.
Koné, Y.J.M., Borges, A., 2008. Dissolved inorganic carbon dynamics in the waters surrounding forested mangroves of the Ca Mau Province (Vietnam). Estuar. Coast. Shelf Sci. 77, 409–421.
Krauss, K., Allen, J., Cahoon, D., 2003. Differential rates of vertical accretion and elevation change among aerial root types in Micronesian mangrove forests. Estuar. Coast. Shelf Sci. 56, 251–259.
Kristensen, E., Alongi, D.M., 2006. Control by fiddler crabs (Uca vocans) and plant roots (Avicennia marina) on carbon, iron, and sulfur biogeochemistry in mangrove sediment. Limnol. Oceanogr. 51, 1557–1571.
Kristensen, E., Suraswadi, P., 2002. Carbon, nitrogen and phosphorus dynamics in creek water of a southeast Asian mangrove forest. Hydrobiologia 474, 197–211.
Kristensen, E., Holmer, M., Banta, G.T., Jensen, M.H., Hansen, K., 1995. Carbon, nitrogen and sulfur cycling in sediments of the Ao Nam Bor mangrove forest, Phuket, Thailand: a review. Phuket Mar. Biol. Cent. Res. Bull. 60, 37–64.
Kroopnick, P., Craig, H., 1972. Atmospheric oxygen: isotopic composition and solubility fractionation. Science 175, 54–55.
Kuenzer, C., Tuan, V.Q., 2013. Assessing the ecosystem services value of Can Gio Mangrove Biosphere Reserve: combining earth-observation- and household-survey-based analyses. Appl. Geogr. 45.
Le, L.T., 2008. Effect of Hydrology on the Structure and Function of Mangrove Ecosystems in the Can Gio Mangrove Biosphere Reserve. (Vietnam).

Lee, S., 1995. Mangrove outwelling: a review. Hydrobiologia 295, 203–212.
Lenton, T.M., Watson, A.J., 2000. Redfield revisited: 2. What regulates the oxygen content of the atmosphere? Glob. Biogeochem. Cycles 14, 249–268.
Leopold, A., Marchand, C., Deborde, J., Allenbach, M., 2017. Water biogeochemistry of a mangrove-dominated estuary under a semi-arid climate (New Caledonia). Estuar. Coasts 40, 773–791.
Linto, N., Barnes, J., Ramachandran, R., Divia, J., Ramachandran, P., Upstill-Goddard, R.C., 2014. Carbon dioxide and methane emissions from mangrove-associated waters of the Andaman Islands, Bay of Bengal. Estuar. Coasts 37, 381–398.
Lu, L., Cheng, H., Pu, X., Liu, X., Cheng, Q., 2015. Nitrate behaviors and source apportionment in an aquatic system from a watershed with intensive agricultural activities. Environ. Sci.: Process. Impacts 17, 131–144.
Maher, D.T., Santos, I.R., Golsby-Smith, L., Gleeson, J., Eyre, B.D., 2013. Groundwater-derived dissolved inorganic and organic carbon exports from a mangrove tidal creek: the missing mangrove carbon sink? Limnol. Oceanogr. 58, 475–488.
Maher, D.T., Sippo, J.Z., Tait, D.R., Holloway, C., Santos, I.R., 2016. Pristine mangrove creek waters are a sink of nitrous oxide. Sci. Rep. 6.
Maher, D.T., Call, M., Santos, I.R., Sanders, C.J., 2018. Beyond burial: lateral exchange is a significant atmospheric carbon sink in mangrove forests. Biol. Lett. 14, 20180200.
Marchand, C., Baltzer, F., Lallier-Verges, E., Alberic, P., 2004. Pore-water chemistry in mangrove sediments: relationship with species composition and developmental stages (French Guiana). Mar. Geol. 208, 361–381.
Marchand, C., Lallier-Verges, E., Baltzer, F., Alberic, P., Cossa, D., Baillif, P., 2006. Heavy metals distribution in mangrove sediments along the mobile coastline of French Guiana. Mar. Chem. 98, 1–17.
Mazda, Y., Kanazawa, N., Wolanski, E., 1995. Tidal asymmetry in mangrove creeks. Hydrobiologia 295, 51–58.
McGroddy, M.E., Daufresne, T., Hedin, L.O., 2004. Scaling of C: N: P stoichiometry in forests worldwide: implications of terrestrial Redfield-type ratios. Ecology 85, 2390–2401.
McKee, K.L., Mendelssohn, I.A., Hester, M.W., 1988. Reexamination of pore water sulfide concentrations and redox potentials near the aerial roots of Rhizophora mangle and Avicennia germinans. Am. J. Bot. 1352–1359.
Middelburg, J.J., Nieuwenhuize, J., Slim, F.J., Ohowa, B., 1996. Sediment biogeochemistry in an East African mangrove forest (Gazi bay, Kenya). Biogeochemistry 34, 133–155.
Molnar, N., Marchand, C., Deborde, J., Patrona, L., Meziane, T., 2014. Seasonal pattern of the biogeochemical properties of mangrove sediments receiving shrimp farm effluents (New Caledonia). J. Aquac. Res. Dev. 5, 262.
Nam, V., Sinh, L., Miyagi, T., Baba, S., Chan, H., 2014. An overview of can Gio District and Mangrove Biosphere Reserve. Studies in Can Gio Mangrove Biosphere Reserve, Ho Chi Minh City, Vietnam Mangrove Ecosystems Techinical Reports. pp. 1–7.
Nordhaus, I., Salewski, T., Jennerjahn, T.C., 2017. Interspecific variations in mangrove leaf litter decomposition are related to labile nitrogenous compounds. Estuar. Coast. Shelf Sci. 192, 137–148.
Odum, E.P., 1968. A research challenge: evaluating the productivity of coastal and estuarine water. In: Proceedings of the 2nd Sea Grant Conference. Graduate School of Oceanography, University of Rhode Island, pp. 63–64.
Odum, W.E., Heald, E.J., 1975. The detritus-based food web of an estuarine mangrove community. Estuar. Res. Chem. Biol. Estuar. Syst. 1, 265.
Ovalle, A., Rezende, C., Lacerda, L., Silva, C., 1990. Factors affecting the hydrochemistry of a mangrove tidal creek, Sepetiba Bay, Brazil. Estuar. Coast. Shelf Sci. 31, 639–650.
Ray, R., Majumder, N., Chowdhury, C., Das, S., Jana, T., 2017. Phosphorus budget of the Sundarban mangrove ecosystem: box model approach. Estuar. Coasts 1–14.
Redfield, A.C., 1958. The biological control of chemical factors in the environment. Am. Sci. 46, 230A–221.
Reef, R., Feller, I.C., Lovelock, C.E., 2010. Nutrition of mangroves. Tree Physiol. 30, 1148–1160.
Rivera Monroy, V.H., De Mutsert, K., Twilley, R.R., Castañeda Moya, E., Romigh, M.M., Davis III, S.E., 2007. Patterns of nutrient exchange in a riverine mangrove forest in the Shark River Estuary, Florida, USA. Hidrobiologica 17.
Saenger, P., Snedaker, S.C., 1993. Pantropical trends in mangrove above-ground biomass and annual litterfall. Oecologia 96, 293–299.
Santos, I.R., Bryan, K.R., Pilditch, C.A., Tait, D.R., 2014. Influence of porewater exchange on nutrient dynamics in two New Zealand estuarine intertidal flats. Mar. Chem. 167, 57–70.
Santos, I.R., Maher, D.T., Larkin, R., Webb, J.R., Sanders, C.J., 2019. Carbon outwelling and outgassing vs. burial in an estuarine tidal creek surrounded by mangrove and saltmarsh wetlands. Limnol. Oceanogr. 64, 996–1013.
Sherman, R.E., Fahey, T.J., Howarth, R.W., 1998. Soil-plant interactions in a neotropical mangrove forest: iron, phosphorus and sulfur dynamics. Oecologia 115, 553–563.
Sigman, D., Casciotti, K., Andreani, M., Barford, C., Galanter, M., Böhlke, J., 2001. A bacterial method for the nitrogen isotopic analysis of nitrate in seawater and freshwater. Anal. Chem. 73, 4145–4153.
Stieglitz, T.C., Clark, J.F., Hancock, G.J., 2013. The mangrove pump: the tidal flushing of animal burrows in a tropical mangrove forest determined from radionuclide budgets. Geochim. Cosmochim. Acta 102, 12–22.
Striggow, B., 2017. Field measurement of oxidation-reduction potential (ORP). In: U.S.E.P (Ed.), Agency.
Subramaniam, A., Yager, P., Carpenter, E., Mahaffey, C., Björkman, K., Cooley, S., Kustka, A., Montoya, J., Sañudo-Wilhelmy, S., Shipe, R., 2008. Amazon River enhances diazotrophy and carbon sequestration in the tropical North Atlantic Ocean. Proc. Natl. Acad. Sci. 105, 10460–10465.
Taillardat, P., Willemsen, P., Marchand, C., Friess, D., Widory, D., Baudron, P., Truong, V.V., Nguyen, T.N., Ziegler, A.D., 2018a. Assessing the contribution of porewater discharge in carbon export and CO 2 evasion in a mangrove tidal creek (Can Gio, Vietnam). J. Hydrol. 563, 303–318.
Taillardat, P., Ziegler, A.D., Friess, D.A., Widory, D., Truong Van, V., David, F., Thành-Nho, N., Marchand, C., 2018b. Carbon dynamics and inconstant porewater input in a mangrove tidal creek over contrasting seasons and tidal amplitudes. Geochim. Cosmochim. Acta 237, 32–48.
Tait, D.R., Maher, D.T., Macklin, P.A., Santos, I.R., 2016. Mangrove pore water exchange across a latitudinal gradient. Geophys. Res. Lett. 43, 3334–3341.
Tait, D.R., Maher, D.T., Sanders, C.J., Santos, I.R., 2017. Radium-derived porewater exchange and dissolved N and P fluxes in mangroves. Geochim. Cosmochim. Acta 200, 295–309.
Tanaka, K., Choo, P.-S., 2000. Influences of nutrient outwelling from the mangrove swamp on the distribution of phytoplankton in the Matang Mangrove Estuary, Malaysia. J. Oceanogr. 56, 69–78.
Trott, L.A., Alongi, D.M., 1999. Variability in surface water chemistry and phytoplankton biomass in two tropical, tidally dominated mangrove creeks. Mar. Freshw. Res. 50, 451–457.
Twilley, R.R., Castañeda-Moya, E., Rivera-Monroy, V.H., Rovai, A., 2017. Productivity and Carbon Dynamics in Mangrove Wetlands, Mangrove Ecosystems: A Global Biogeographic Perspective. Springer, pp. 113–162.
UN, 2014. World Urbanization Prospects: The 2014 Revision, Highlights. Department of Economic and Social Affairs. Population Division, United Nations.
Van Vinh, T., Marchand, C., Linh, T.V.K., Vinh, D.D., Allenbach, M., 2019. Allometric models to estimate above-ground biomass and carbon stocks in Rhizophora apiculata tropical managed mangrove forests (Southern Viet Nam). For. Ecol. Manag. 434, 131–141.
Vazquez, P., Holguin, G., Puente, M., Lopez-Cortes, A., Bashan, Y., 2000. Phosphate-solubilizing microorganisms associated with the rhizosphere of mangroves in a semiarid coastal lagoon. Biol. Fertil. Soils 30, 460–468.
Vonk, J.A., Middelburg, J.J., Stapel, J., Bouma, T.J., 2008. Dissolved organic nitrogen uptake by seagrasses. Limnol. Oceanogr. 53, 542–548.
Wang, F., Chen, N., Yan, J., Lin, J., Guo, W., Cheng, P., Liu, Q., Huang, B., Tian, Y., 2019. Major processes shaping mangroves as inorganic nitrogen sources or sinks: insights from a multidisciplinary study. J. Geophys. Res. Biogeosci. 124.
Wankel, S.D., Kendall, C., Paytan, A., 2009. Using nitrate dual isotopic composition (δ15N and δ18O) as a tool for exploring sources and cycling of nitrate in an estuarine system: Elkhorn Slough, California. J. Geophys. Res.: Biogeosci. 114.
Wolanski, E., Jones, M., Bunt, J., 1980. Hydrodynamics of a tidal creek-mangrove swamp system. Mar. Freshw. Res. 31, 431–450.
Xiao, K., Wu, J., Li, H., Hong, Y., Wilson, A., Jiao, J., Shananan, M., 2018. Nitrogen fate in a subtropical mangrove swamp: potential association with seawater-groundwater exchange. Sci. Total Environ. 635, 586–597.
Xue, D., Boeckx, P., Wang, Z., 2014. Nitrate sources and dynamics in a salinized river and estuary–a δ 15 N–NO 3 − and δ 18 O–NO 3 − isotope approach. Biogeosciences 11, 5957–5967.
Zehr, J.P., Kudela, R.M., 2011. Nitrogen cycle of the open ocean: from genes to ecosystems. Annu. Rev. Mar. Sci. 3, 197–225.